RSC Advances

PAPER

View Article Online
View Journal | View Issue

Cite this: *RSC Adv.*, 2026, **16**, 22897

Cooperative supramolecular integration of QS-21 into polymeric micelles as a tunable nanoadjuvant platform for subunit vaccines

Patricio Guillermo Márquez, [ab] Leonardo Gabriel Alonso, [ab] Juan Ignacio Marfía, [cd] Ignacio Smith, [ae] Ana Carolina Mourelle, [cd] María Lina Formica, [f] María Victoria Miranda, [ab] Silvina Noemí Valdez, [cd] Federico Javier Wolman [ab] and Romina Julieta Glisoni *[ab]

Potent saponin adjuvants such as QS-21, used in clinically approved vaccine formulations, remain limited by intrinsic hemolytic activity and restricted aqueous stability, motivating biomaterials strategies aimed at regulating their interfacial behavior while preserving immunostimulatory function. Here, we show that when combined with amphiphilic PEO–PPO triblock copolymers (P123 and F127), QS-21 appears to participate in cooperative supramolecular integration into polymeric micelles rather than behaving as a passively encapsulated cargo. This architecture-dependent organization gives rise to structurally coherent nanosystems with enhanced dilution stability and controlled membrane activity. Comparative analysis revealed that P123/QS-21 assemblies form compact, monodisperse micelles (~21 nm) with marked resistance to dilution, whereas F127-based systems display greater structural heterogeneity and reduced supramolecular robustness. Cooperative integration is associated with attenuation of hemolytic activity in a concentration-dependent manner relative to free QS-21 while preserving functional accessibility, consistent with controlled interfacial presentation of the saponin. These physicochemical features are supported by DLS, TEM, and NTA analyses. *In vivo* evaluation using a SARS-CoV-2 Spike subunit antigen indicates that P123/QS-21 is associated with enhanced systemic and mucosal antibody responses while inducing functional neutralizing activity. Together, these findings support cooperative supramolecular integration as a biomaterials design principle to modulate membrane activity and nanoadjuvant performance, providing a scalable and tunable framework for the development of subunit vaccine platforms.

Received 5th March 2026
Accepted 26th April 2026

DOI: 10.1039/d6ra01909a

rsc.li/rsc-advances

1. Introduction

Vaccines are biological preparations that induce protective immune responses and have significantly reduced the global burden of infectious diseases.[1–3] Conventional platforms based on killed or live-attenuated microorganisms provide intrinsic immunostimulatory cues but may involve poorly defined components and safety concerns, particularly in immunocompromised individuals.[4–6]

In contrast, subunit vaccines based on purified antigens offer improved safety and manufacturing flexibility. However, their reduced intrinsic immunogenicity often results in weaker and shorter-lived immune responses.[4,6,7] Consequently, the inclusion of effective adjuvants is required to achieve robust and durable protection.[4,5,8]

Adjuvants enhance the magnitude and quality of vaccine-induced immune responses and are broadly classified as immunostimulatory or delivery-type systems.[9] Immunostimulatory adjuvants activate innate immune pathways through pattern-recognition receptors (PRRs) on antigen-presenting cells (APCs).[10,11] Delivery-type adjuvants improve antigen and/or immunostimulant presentation by acting as carriers, depots, or stabilizing matrices, and include aluminum salts, liposomes, lipid nanoparticles (LNPs), polymeric nanoparticles, emulsions, virus-like particles (VLPs), and immune-stimulating

[a]*Universidad de Buenos Aires (UBA), Facultad de Farmacia y Bioquímica, Departamento de Microbiología, Inmunología, Biotecnología y Genética, Cátedra de Biotecnología, Junín 956, C1113AAD Buenos Aires, Argentina*

[b]*UBA-CONICET, Facultad de Farmacia y Bioquímica, Instituto de Nanobiotecnología (NANOBIOTEC), Junín 956, Buenos Aires, C1113AAD, Argentina. E-mail: rglisoni@ffyb.uba.ar; romy.glisoni@gmail.com; Tel: +54 11 5287 4682*

[c]*Universidad de Buenos Aires (UBA), Facultad de Farmacia y Bioquímica, Departamento de Microbiología, Inmunología, Biotecnología y Genética, Cátedra de Inmunología, Junín 956, C1113AAD Buenos Aires, Argentina*

[d]*UBA-CONICET, Facultad de Farmacia y Bioquímica, Instituto de Estudios de la Inmunidad Humoral "Prof. Ricardo A. Margni" (IDEHU), Buenos Aires, Argentina*

[e]*Trebe Biotech SRL, Ruta 8 km 225.5, Pergamino, Buenos Aires, Argentina*

[f]*Unidad de Investigación y Desarrollo en Tecnología Farmacéutica (UNITEFA), CONICET, Departamento de Ciencias Farmacéuticas, Facultad de Ciencias Químicas, Universidad Nacional de Córdoba, Ciudad Universitaria, Córdoba 5000, Argentina*

complexes (ISCOMs).[5,9,12] Accordingly, an increasing number of FDA- and EMA-approved vaccines incorporate nanoparticulate or nanostructured components that promote efficient uptake by immune cells, antigen stabilization, and controlled antigen trafficking.[9,13–18] Importantly, several of these systems can also display intrinsic immunostimulatory activity, further contributing to their overall adjuvant effect.[19–22]

Within this context, amphiphilic block copolymers composed of poly(ethylene oxide) (PEO) and poly(propylene oxide) (PPO), commonly referred to as poloxamers (and poloxamines when combined with ethylenediamine cores), represent a widely studied class of biomaterials in pharmaceutical formulations.[23–31] These copolymers are available across a wide range of molecular weights and hydrophilic–lipophilic balance (HLB) values, enabling precise control over their physicochemical behavior.[23–31] Depending on polymer architecture, concentration, and temperature, PEO–PPO copolymers can self-assemble into polymeric micelles (PMs) above a critical micelle concentration (CMC) or form thermoresponsive hydrogels at higher concentrations, offering formulation strategies that span nanoscale carriers to injectable depots.[23–31]

Beyond their classical role as inert delivery materials, increasing evidence indicates that PEO–PPO copolymers can contribute to vaccine performance by stabilizing labile antigens, facilitating antigen delivery, and, in some cases, promoting innate immune activation.[32–41] Notably, the predictable and programmable self-assembly of these copolymers provides an opportunity to engineer cooperative nanosystems in which immunostimulatory molecules could participate directly in the assembly process. Such systems give rise to emergent physicochemical and biological properties that are not readily achieved through passive encapsulation alone.

Saponins are natural amphiphilic glycosides, most prominently derived from *Quillaja saponaria*, with potent immunomodulatory activity and a long history of investigation as vaccine adjuvants.[42,43] Among these, Quil A, a heterogeneous mixture of saponins extracted from *Quillaja saponaria* bark, has been extensively studied in the context of vaccination. These saponins elicit robust humoral and cellular immune responses, promoting both T helper 1 (Th1) and T helper 2 (Th2) immunity as well as cytotoxic T-lymphocyte (CTL) activation, making them particularly attractive for subunit vaccines.[42,43]

QS-21, a highly purified saponin fraction originally isolated from Quil A, is among the most potent saponin-based adjuvants currently employed and is incorporated into licensed vaccines targeting herpes zoster and respiratory syncytial virus, as well as a broad range of clinical-stage formulations.[43–50] QS-21 is also widely used in combination with monophosphoryl lipid A (MPL) and other immune stimulants, including liposomal formulations developed for specific vaccination programs.[50–53] This combination exhibits well-documented synergy in enhancing both innate and adaptive immune responses.[54]

From a structural standpoint, QS-21 comprises a hydrophobic quillaic acid triterpene aglycone, a fatty acyl chain, and hydrophilic oligosaccharide domains that together confer amphiphilicity and underpin its biological activity (Fig. 1a).[43,55–58] These features enable interactions with cholesterol-rich membranes and have been associated with lysosomal destabilization and enhanced antigen cross-presentation, mechanisms that contribute to its strong cellular immunogenicity.[43,55,56] At the same time, this amphiphilic architecture also underlies major formulation challenges. QS-21 is intrinsically hemolytic and exhibits limited aqueous stability, restricting its broader deployment.[43,57,58] Current formulation strategies largely rely on cholesterol-containing liposomes and ISCOM-like structures to mitigate QS-21 hemotoxicity; however, these approaches primarily focus on stabilization within lipid-based assemblies, while the potential contribution of QS-21 to supramolecular organization is less explicitly addressed. Moreover, they often depend on high-purity lipid components and multi-step, scale-sensitive manufacturing processes that can limit cost-effectiveness and scalability.[44–47]

Importantly, complete sequestration of immunostimulatory molecules may not always be desirable, as partial exposure and dynamic accessibility of active motifs may be required to preserve biological function.[59] This highlights the need for formulation strategies that enable controlled and concentration-dependent modulation of QS-21 interactions with biological membranes, rather than simple encapsulation or shielding.

Despite the established potency of QS-21, copolymer-based nanoplatforms in which the saponin actively contributes to nanoscale organization remain largely unexplored. Leveraging the intrinsic amphiphilicity of QS-21 together with the programmable self-assembly of PEO–PPO block copolymers offers an opportunity to establish a distinct nanoadjuvant design paradigm, enabling fine control over interfacial organization, dilution stability, and biological activity.

In this work, we introduce a hybrid nanoadjuvant platform based on the cooperative supramolecular integration of QS-21 with PEO–PPO triblock copolymers, using P123 and F127 as representative architectures with distinct hydrophilic–hydrophobic balance and self-assembly behavior. In this context, QS-21 is proposed to contribute as a structural component within mixed PMs through cooperative supramolecular interactions. This integration is expected to influence nanoscale organization, dilution stability, and membrane activity. By contrasting P123 and F127 systems, we aim to evaluate copolymer architecture as a key design parameter for cooperative copolymer–saponin integration and downstream immunological outcomes. Collectively, this work supports supramolecular integration as a potential biomaterials design principle for controlling the safety and functional accessibility of membrane-active immunomodulators.

2. Experimental

2.1 Materials

All chemicals and reagents were used as received, without further purification. Linear PEO–PPO–PEO triblock copolymers, Pluronic® P123 (average molecular weight (M_w) ~ 5800 g mol^{-1}; PEO content = 30 wt%) and Pluronic® F127 (M_w ~ 12 600 g mol^{-1}; PEO content = 70 wt%), as well as QS-21 saponin (extracted from *Quillaja saponaria*; M_w ~ 1990 g mol^{-1}), were

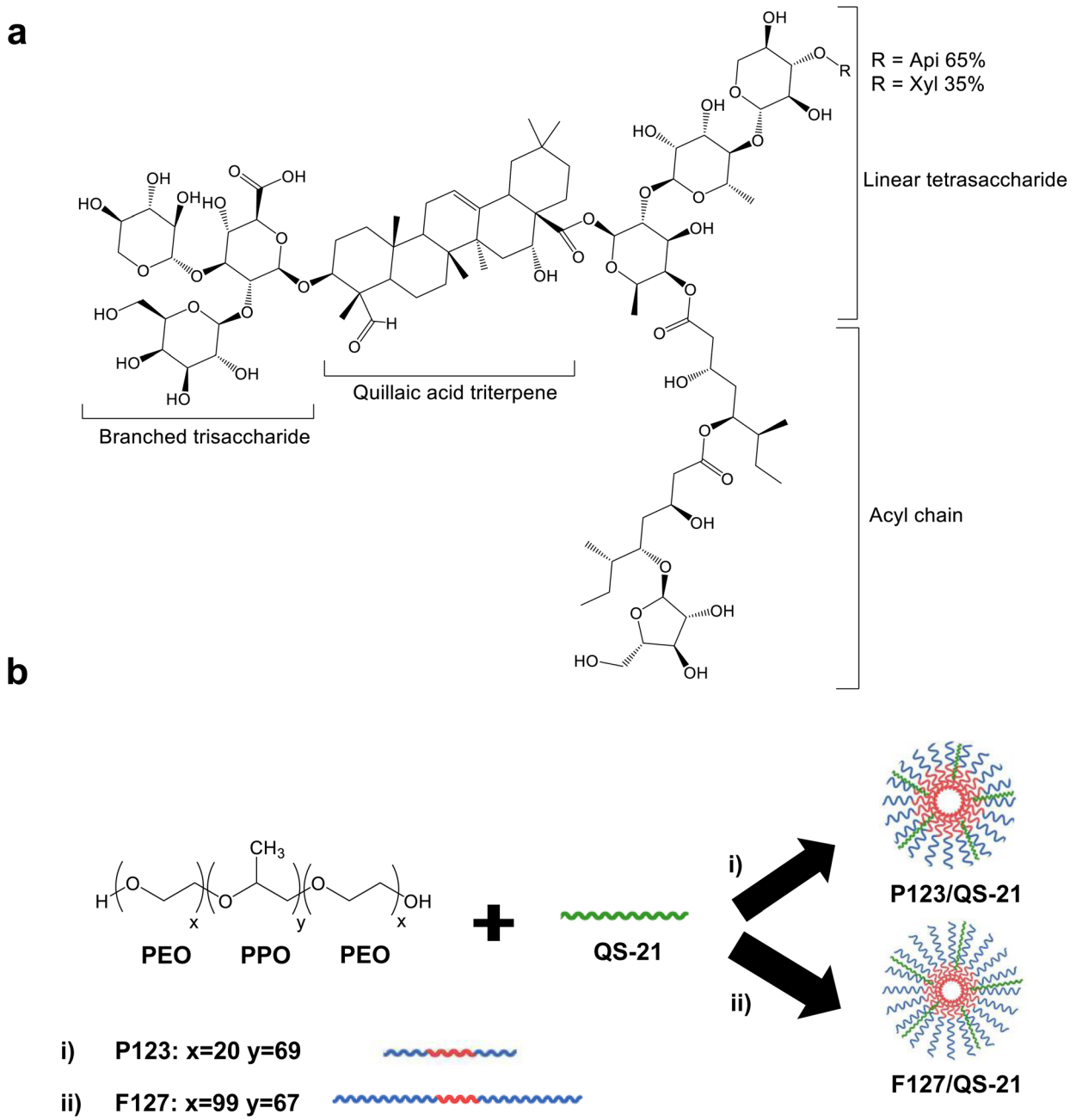

Fig. 1 Structural basis and cooperative self-assembly of QS-21 with PEO–PPO block copolymers. (a) Chemical structure of QS-21 highlighting its amphiphilic architecture, including hydrophobic domains (quillaic acid triterpene aglycone and acyl chain) and hydrophilic oligosaccharide moieties. (b) Schematic representation of cooperative interactions between QS-21 and PEO–PPO block copolymers (P123 and F127) leading to the formation of mixed polymeric micelles (PMs): (i) P123/QS-21 and (ii) F127/QS-21.

purchased from Sigma-Aldrich (Argentina). Recombinant trimeric SARS-CoV-2 Spike protein (approximate molecular weight ~550 kDa, including glycosylation; lyophilized powder) was supplied by Trebe Biotech SRL (Pergamino, Buenos Aires, Argentina). Stabilized sterile ovine blood was obtained from Laboratorio Alfredo C. Gutiérrez (Buenos Aires, Argentina) and stored at 4 °C until use. For ELISA assays, phosphate-buffered saline (PBS) was used as coating buffer; 3% (w/v) skim milk in PBS as blocking buffer; and PBS containing 0.05% (v/v) Tween 20 (PBS-T) as washing buffer. Reagent dilutions were prepared in PBS-T supplemented with 3% (w/v) skim milk (PBS-MT). Streptavidin–horseradish peroxidase was purchased from Jackson ImmunoResearch Laboratories (West Grove, PA, USA), and the 3,3′,5,5′-tetramethylbenzidine (TMB)/H_2O_2 single-component substrate kit was obtained from Bio-Rad (Hercules, CA, USA).

2.2 Preparation of single and mixed polymeric micelles

Single polymeric micelles (single PMs), composed exclusively of pristine PEO–PPO block copolymers (P123 or F127), were

prepared at concentrations ranging from 0.5 to 10% (w/v) in PBS, as previously described by our group.[23–27] Briefly, the required amount of copolymer was weighed and hydrated by adding PBS (pH 7.2) at room temperature (RT). PBS was prepared using ultrapure water (18 MΩ cm) obtained from a Milli-Q purification system (Millipore, USA). Dispersions were gently mixed until homogeneous and stored overnight at 4 °C to ensure complete hydration and equilibration. On the following day, samples were equilibrated at RT and adjusted to the final volume to reach the target copolymer concentration.

QS-21 stock dispersions (0.2% w/v) were prepared by dispersing QS-21 in PBS under gentle mixing until visually homogeneous, followed by adjustment to the final volume. Working dilutions spanning QS-21 concentrations from 0.0013 to 0.16% (w/v) were subsequently prepared and used across the different physicochemical and biological assays described in this study.

Mixed PMs were prepared by hydrating the required amount of P123 or F127 directly with an appropriate volume of QS-21 dispersion, followed by adjustment to the final volume with PBS. Formulations were stored overnight at 4 °C to promote copolymer hydration and potential cooperative interactions between QS-21 and the copolymer, and were subsequently equilibrated at RT prior to analysis. Mixed PMs were denoted as P123/QS-21 and F127/QS-21, respectively. For antigen-adjuvant compatibility studies, lyophilized SARS-CoV-2 Spike protein was reconstituted directly in PBS or in pre-formed P123/QS-21 dispersions to reach a final Spike concentration of 0.07 mg mL^{-1}, corresponding to the concentration used in the *in vivo* immunization studies. Formulations were gently mixed prior to physicochemical characterization. Unless otherwise stated, micellar formulations were prepared fresh prior to physicochemical characterization and biological experiments. No filtration was applied in order to preserve the self-assembled structures; all solutions were prepared using sterile PBS and handled under clean conditions.

2.3 Physicochemical characterization

Physicochemical characterization was performed to evaluate micellar self-assembly, nanoscale organization, stability under dilution, and the impact of QS-21 incorporation. Copolymer concentrations were selected to ensure consistency across techniques while allowing complementary interrogation of fully assembled micellar populations and near-CMC assembly regimes.

2.3.1 Hydrodynamic diameter and polydispersity by dynamic light scattering (DLS). DLS measurements were performed for single PMs (P123 and F127), free QS-21, and mixed PMs (P123/QS-21 and F127/QS-21) at the concentrations indicated in Section 2.2. Size and dispersity analyses were conducted at copolymer concentrations (typically 2.5% w/v) well above their respective apparent CMC values to ensure fully assembled micellar populations and reliable ensemble-averaged measurements.

Measurements were carried out at 25 and 37 °C in PBS using a Zetasizer Nano ZS (Malvern Instruments, UK) equipped with a 633 nm He–Ne laser and a digital correlator (model ZEN3600) operating at a backscattering detection angle of 173° and fixed position (4.65 mm). For each formulation, three independently prepared samples were analyzed, with at least six consecutive runs recorded per sample. Hydrodynamic diameter (D_h) and polydispersity index (PDI) were obtained using Zetasizer software (v7.13) and are reported as mean ± standard deviation (±S.D.). Instrument performance was verified using polystyrene latex nanosphere standards (NIST 3020A and 3400A, Thermo Scientific) measured under identical experimental conditions.

To assess antigen compatibility, DLS measurements were additionally performed on the antigen control (Spike PBS) and on Spike protein formulated with P123/QS-21 mixed micelles (P123/QS-21/Spike) at 25 and 37 °C without prior filtration. This experimental design was intended to evaluate antigen–adjuvant compatibility and preservation of micellar nanoscale organization rather than antigen encapsulation efficiency.

2.3.2 Apparent critical micelle concentration (CMC) by DLS-derived scattering. Experimental apparent CMC values for single PMs, mixed PMs, and free QS-21 dispersions were determined in PBS at 37 °C by monitoring the derived count rate (DCR) using DLS (Zetasizer Nano ZS, Malvern Instruments) at a scattering angle of 173°, following an approach previously established by our group.[23,25,29] Accordingly, the CMC values reported here should be regarded as apparent CMCs, derived from changes in scattering behavior and reflecting the onset of stable nanoscale assemblies.

Stock dispersions of pristine and mixed PMs were serially diluted to obtain final copolymer concentrations in the range of 0.001–5% (w/v), while QS-21 dispersions were evaluated over the concentration range of 0.0013–0.64% (w/v). All measurements were performed after thermal equilibration at 37 °C. These dilution conditions were specifically selected to probe micellar assembly close to the critical concentration. DCR values (kcps) were plotted as a function of the logarithm of concentration ($\log_{10}$), and the apparent CMC was defined as the concentration at which an abrupt increase in scattering intensity, corresponding to an inflection point in the DCR profile, was observed.[23,25,29]

2.3.3 Morphology by negative staining transmission electron microscopy (TEM). TEM analyses were performed on free QS-21, representative single PMs (P123), and mixed PMs (P123/QS-21) at concentrations corresponding to those used for DLS measurements. Samples prepared as described in Section 2.2 were deposited onto ultrathin carbon-coated QUANTIFOIL holey copper grids (200 mesh), incubated for 1 h at 37 °C, negatively stained with 2% (w/v) phosphotungstic acid for 60 s, air-dried at RT, and imaged using a JEOL JEM-1010 transmission electron microscope (JEOL, Tokyo, Japan). TEM imaging was performed on dried samples and therefore provides qualitative morphological information complementary to hydrodynamic measurements.

2.3.4 Particle concentration by nanoparticle tracking analysis (NTA) and zeta potential. Particle concentration and zeta potential were determined using a ZetaView PMX-230 Twin Laser system (Particle Metrix, Germany) in PBS at 25 °C. Measurements were performed for single PMs (P123 and F127)

and mixed PMs (P123/QS-21 and F127/QS-21). Instrument calibration was verified prior to analysis using polystyrene latex nanosphere standards (NIST 3020A and 3400A, Thermo Scientific). Particle size distribution and concentration were obtained in scatter mode using a 488 nm laser, while zeta potential was determined in electrophoresis mode. Measurements were recorded at 11 positions per sample. Samples were diluted in PBS using dilution factors of 1 : 10 000 for P123-based systems and 1 : 100 for F127-based systems to ensure optimal particle tracking.

Zeta potential measurements were performed under the same dilution conditions used for NTA for each formulation. Conductivity was checked prior to electrophoretic measurements and adjusted when necessary to enable comparative assessment of interfacial changes upon QS-21 incorporation. Data acquisition and analysis were performed using ZetaView software (version 8.05.16 SP7, Particle Metrix, Germany). Representative NTA videos of P123/QS-21 and F127/QS-21 mixed PMs (SI Videos S1 and S2) were recorded during particle-tracking measurements and exported directly from ZetaView software without post-processing.

2.3.5 Microenvironmental fluorescence probing and comparative analysis. Fluorescence measurements were performed using fluorescein free acid (M_w 332.31 g mol^{-1}, Sigma-Aldrich, Argentina) as a microenvironment-sensitive probe. Analyses were carried out using a Tecan Infinite 200 PRO microplate reader (Tecan Austria GmbH) with black 96-well plates (200 μL final volume per well). Measurements were conducted at 37 °C after 30 min incubation under controlled temperature conditions. Prior to reading, samples were subjected to orbital shaking (15 s) followed by equilibration (30 s). All experiments were performed using three independently prepared samples, each measured in triplicate ($n = 3$).

A fluorescein stock solution was prepared in DMSO and diluted in PBS (pH 7.2) to a final concentration of 0.5 μM. QS-21 stock solutions and copolymer dispersions (P123 and F127, 2.5% w/v), as well as mixed systems, were prepared as described in Section 2.2. Serial dilutions were performed to obtain QS-21 concentrations ranging from 0.005 to 0.64% w/v, while maintaining constant copolymer and fluorescein concentrations across all samples. Corresponding control formulations without fluorescein were prepared under identical conditions. This experimental design isolates the effect of QS-21 under constant probe and copolymer conditions, comparison with theoretical additive responses based on the assumption of independent contributions of QS-21 and the copolymer as a reference model.

Fluorescence data were corrected by subtracting the corresponding blank ($F_{corr} = F_{sample} - F_{blank}$). Relative fluorescence intensity (F_{rel} intensity) was calculated as defined in eqn (1):

$$F_{rel}\ \text{intensity} = F_{corr}(\text{QS-21}_x)/F_{corr}(\text{QS-21}_0) \quad (1)$$

where $F_{corr}(\text{QS-21}_0)$ corresponds to the copolymer–fluorescein formulation in the absence of QS-21. Results were expressed as F_{rel} intensity as a function of QS-21 concentration (% w/v).

Theoretical additive fluorescence responses were calculated from the individual contributions of copolymer-only and QS-21-only systems and compared with the corresponding experimental values to identify deviations from the assumption of independent partitioning behavior.

2.4 Hemolysis assay and concentration-dependent modulation of QS-21 activity

In vitro hemolytic activity was evaluated for pristine PEO–PPO PMs, mixed QS-21 and PEO–PPO PMs, and free QS-21 following standard protocols with minor modifications.[60] A standardized 5% (v/v) red blood cell suspension (RBC 5%), prepared from stabilized sterile ovine blood, was used in all assays. Red blood cells were isolated by centrifugation, washed with PBS, and adjusted to the target concentration based on hemoglobin absorbance at 405 nm, as previously described.[60]

Hemolysis assays were performed by incubating three volumes of RBC 5% with one volume of each test formulation (final volume 500 μL) at 37 °C for 30 min. Unless otherwise stated, all copolymer and QS-21 concentrations refer to final concentrations in the incubation mixture. QS-21 (0.16% w/v; $n = 6$) was used as the positive control (defined as 100% hemolysis), while RBC 5% in PBS ($n = 6$) served as the negative control.

To assess the contribution of formulation variables to hemolytic activity, pristine copolymers (P123 and F127) were evaluated over a broad concentration range (0.5–2.5% w/v). Mixed copolymer formulations containing different P123 : F127 ratios were also tested at selected concentrations. For free QS-21 and QS-21 containing systems, hemolysis was evaluated as a function of QS-21 concentration (0.0013–0.16% w/v). For mixed formulations, fixed copolymer concentrations were used (P123 at 0.5% w/v and F127 at 1.25% w/v). These copolymer concentrations were selected based on colloidal stability considerations and to provide a conservative *in vitro* assessment, taking into account our previous experience with copolymer concentrations commonly employed in cell-based assays.[23,24] Higher copolymer concentrations were subsequently used *in vivo*, as permitted by the larger injection volumes and physiological dilution conditions associated with *in vivo* administration.[25]

Following incubation, samples were centrifuged at 2000 × *g* for 10 min at RT. Released hemoglobin in the supernatant was quantified by diluting 10 μL of supernatant in 90 μL PBS (1 : 10) in a 96-well plate, and absorbance was measured at 405 nm using a microplate reader (Multiskan FC, Thermo Scientific Labsystems, USA). Percent hemolysis was calculated after background subtraction and expressed relative to the positive control according to eqn (2):

$$\%\ \text{Hemolysis} = 100 \times [(\text{Abs sample} - \text{Abs NC})/(\text{Abs PC} - \text{Abs NC})] \quad (2)$$

where Abs sample is the absorbance of the test sample, Abs NC corresponds to the negative control (RBC 5% in PBS), and Abs PC corresponds to the positive control (QS-21, 100% hemolysis).

2.5 *In vivo* immunization and immunological evaluation

2.5.1 Animals. All animal procedures were approved by the Institutional Committee for the Care and Use of Laboratory Animals (CICUAL) of the Facultad de Farmacia y Bioquímica, Universidad de Buenos Aires (FFyB-UBA) (REDEC-2021-2112-E-UBA-DCT FFYB), and were conducted in accordance with institutional and national guidelines. Female Sprague-Dawley rats (6–8 weeks old) were obtained from the FFyB-UBA Animal Facility (Bioterio) (Buenos Aires, Argentina) and housed in individually ventilated cages (two rats per cage) under controlled environmental conditions (22 ± 2 °C; 50–60% relative humidity; 12 h light/dark cycle), with ad libitum access to standard chow and water. Body weights ranged from 180 to 260 g during the experimental period. Animals were randomly assigned to experimental groups prior to immunization. Investigators performing immunological readouts and data processing were blinded to group allocation during sample processing and data analysis when feasible. Animals were monitored daily for general health status, signs of distress, and potential adverse reactions at the injection site.

2.5.2 Immunization protocol. Intramuscular administration was selected as a clinically relevant route.[61–63] Animals were randomly assigned to three experimental groups: (i) group 1 (adjuvant control: P123/QS-21), (ii) group 2 (antigen control: Spike PBS), and (iii) group 3 (Spike/adjuvant: P123/QS-21/Spike). Each group received four intramuscular (IM) injections on days 1, 14, 35, and 95. Injections were administered into the quadriceps muscle, alternating between left and right quadriceps at each immunization. Groups 2 and 3 each included six animals ($n = 6$), whereas group 1 included three animals. Recombinant SARS-CoV-2 Spike protein was administered at a dose of 10 μg per injection in a final inoculation volume of 150 μL. The adjuvant formulation consisted of P123/QS-21 at 2.5/0.02% (w/v) in PBS. Lyophilized Spike protein was reconstituted either in PBS (group 2) or directly in the adjuvant dispersion (group 3) to reach the target antigen concentration. Group 1 received the adjuvant formulation alone.

P123/QS-21 formulations were prepared as described in Section 2.2, aliquoted, and stored at −80 °C to preserve formulation integrity until administration. Samples were thawed immediately prior to injection and used within the same experimental session; repeated freeze–thaw cycles were avoided. No animals were excluded from the analysis. Group sizes were selected based on an exploratory preclinical study design and practical constraints commonly applied in early-stage immunogenicity studies. Blood and bronchoalveolar lavage (BAL) samples were collected at the indicated time points under deep anesthesia, in accordance with institutional animal welfare guidelines. The P123/QS-21 composition selected for *in vivo* studies (2.5/0.02% w/v) was rationally defined based on physicochemical and biological considerations. At this composition, P123 remains well above the apparent CMC, ensuring micellar integrity upon dilution, while QS-21 is present within a concentration window that enables efficient cooperative assembly and partial attenuation of hemolytic activity. This formulation also accounts for the estimated dilution occurring at the injection site, thereby maintaining nanoscale stability while preserving adjuvant function.

2.5.3 SARS-CoV-2 antibody detection by bridge ELISA (b-ELISA). SARS-CoV-2-specific antibodies were quantified using a bridge ELISA (b-ELISA) as previously described by Trabucchi *et al.*, with minor modifications.[62] MaxiSorp microplates (Nunc, Roskilde, Denmark) were coated overnight at 4 °C with purified Spike protein (2 μg mL^{-1} in PBS; 50 μL per well). Plates were washed three times with PBS, blocked for 1 h with 200 μL blocking buffer (3% skim milk in PBS), and washed six times with PBS-T. Serum and BAL samples were analyzed in duplicate. Samples were added to the plates and incubated for 20 min at RT. Plates were then washed six times with PBS-T, followed by the addition of biotinylated Spike protein (50 ng per well). After 20 min of incubation, plates were washed six times with PBS-T, and bound biotinylated Spike protein was detected using streptavidin–horseradish peroxidase (1 : 300). Plates were incubated for 20 min at 37 °C, washed five times with PBS-T, and subjected to a final wash with PBS (200 μL). TMB substrate was added and incubated for 15 min in the dark, and the reaction was stopped with 4 N H_2SO_4. Absorbance was read at 450 nm using a Multiskan FC plate reader (Thermo Scientific Labsystems, USA). Blank controls were included by replacing serum or BAL samples with PBS-MT. Hyperimmune equine anti-Spike serum was used as a positive control.

Results were expressed as specific absorbance (A), calculated as $A_{\text{sample}} - A_{\text{blank}}$, and converted to a positivity index (PI) according to eqn (3):

$$\text{PI} = 100 \times A_{\text{sample}}/A_{\text{positive control}} \quad (3)$$

where A_{sample} and $A_{\text{positive control}}$ correspond to blank-corrected absorbance values. The cut-off for positivity was set at PI = 5.0.

2.5.4 Surrogate virus neutralization test (sVNT). Neutralizing antibodies were assessed using a surrogate virus neutralization test (sVNT) based on inhibition of the ACE2–RBD interaction. Briefly, 96-well microplates were coated overnight at 4 °C with recombinant human ACE2 (2 μg mL^{-1} in PBS, 50 μL per well). Plates were washed with PBS-T and blocked with 3% (w/v) skim milk in PBS for 1 h at RT. Serum samples (and BAL, when indicated) were heat-inactivated (56 °C, 30 min) and serially diluted in PBS-MT. Samples were pre-incubated for 30 min at 37 °C with a fixed amount of biotinylated (or horseradish peroxidase (HRP)-conjugated) SARS-CoV-2 RBD and then transferred to ACE2-coated wells (50 μL per well). After 30 min at 37 °C, plates were washed and bound RBD was detected using streptavidin–HRP (when biotin–RBD was used) or directly by TMB development (when HRP–RBD was used). Both detection formats yielded comparable inhibition profiles and were analyzed using the same calculation criteria. Absorbance was read at 450 nm. Percent inhibition of the ACE2–RBD interaction was calculated according to eqn (4):

$$\%\ \text{Inhibition} = 100 \times [1 - (\text{Abs sample}/\text{Abs NC})] \quad (4)$$

where Abs NC corresponds to wells containing RBD without serum (0% inhibition). Neutralization titers were expressed as

ID_{50} values (sample dilution yielding 50% inhibition), obtained by nonlinear regression of inhibition curves.

2.6 Statistical analysis

Statistical analyses were performed using one-way or two-way analysis of variance (ANOVA), followed by Bonferroni's post hoc multiple-comparison test, as appropriate for each dataset. Differences were considered statistically significant at $p < 0.05$, with thresholds of $p < 0.01$, $p < 0.001$ and $p < 0.0001$ indicated where applicable, while ns denotes non-significant differences. Statistical annotations are specified in the corresponding figure legends. Analyses were conducted using Minitab Statistical Software v22.1 (Minitab Inc., State College, PA, USA) and GraphPad Prism v9 (GraphPad Software, Inc., San Diego, CA, USA). Data are presented as mean ± standard deviation unless otherwise indicated.

3. Results and discussion

The cooperative self-assembly of QS-21 with PEO–PPO triblock copolymers gave rise to hybrid nanoadjuvant systems in which supramolecular organization, dilution stability, membrane activity, and *in vivo* adjuvant performance were influenced by copolymer architecture. Rather than redistributing within preformed micellar domains, QS-21 appears to contribute to the supramolecular organization of mixed PMs, giving rise to emergent physicochemical and biological properties. Importantly, this work suggests that polymer architecture may function as a supramolecular design parameter to modulate the interfacial activity and immunological output of QS-21 within polymeric nanostructures.

We first examined how copolymer–saponin interactions influence nanoscale organization and resistance to dilution in P123- and F127-based systems. Incorporation of QS-21 into the micellar framework was found to modulate structural parameters and QS-21-associated membrane activity while maintaining colloidal integrity, revealing copolymer-dependent differences in supramolecular robustness. These physicochemical features were subsequently correlated with the biological evaluation. By integrating nanoscale characterization with *in vivo* immunogenicity studies, we explore a structure–function relationship in which cooperative supramolecular integration may contribute to the safety profile and adjuvant output of QS-21. Collectively, this section supports cooperative copolymer–saponin assembly as a potential biomaterials design strategy for controlling membrane-active immunomodulators within nanostructured vaccine platforms.

3.1 Cooperative self-assembly and physicochemical organization of pristine and QS-21-containing PMs

Single PMs based on PEO–PPO triblock copolymers (P123 and F127), mixed PMs incorporating QS-21 (P123/QS-21 and F127/QS-21), and free QS-21 dispersions were prepared as described in Section 2.2. A schematic representation of the proposed cooperative interactions between QS-21 and PMs is presented in Fig. 1b.

Owing to its amphiphilic architecture (Fig. 1a), QS-21 is proposed to interact through hydrophobic contributions of its acyl chain within PPO-rich micellar domains, while the triterpenoid scaffold and hydrophilic oligosaccharide moieties remain oriented toward the micellar interface and corona, where they can interact with PEO chains and the surrounding aqueous environment. The lipophilic acyl chain of QS-21 represents the most hydrophobic and conformationally flexible region of the molecule, making it a plausible anchoring element for interaction with the hydrophobic PPO-rich micellar domains of PMs.[48,55,58] This spatial organization is consistent with interfacial localization of QS-21 within the micellar architecture and supports a cooperative self-assembly process in which the saponin participates in the supramolecular organization of the mixed assemblies.

Although P123 and F127 share comparable hydrophobic PPO block lengths, they differ markedly in PEO content and hydrophilic–lipophilic balance (HLB ≈ 7–9 for P123; HLB ≈ 18–23 for F127).[23–27] The lower PEO fraction of P123 is expected to promote a more compact and less hydrated micellar corona, with increased exposure of the PPO–PEO interfacial region, whereas F127 forms a highly hydrated and sterically extended shell.

These architecture-dependent differences in corona hydration and interfacial packing are anticipated to modulate the cooperative integration and interfacial positioning of amphiphilic QS-21 molecules, thereby influencing nanoscale organization, interfacial accessibility, and assembly stability. By contrasting these two copolymer architectures, we propose a framework to interrogate how supramolecular organization may influence the physicochemical robustness of mixed PMs and sets the stage for subsequent evaluation of membrane activity and adjuvant performance.

3.1.1 Hydrodynamic diameter and size dispersity. DLS analysis indicated efficient cooperative self-assembly between P123 PMs (2.5% w/v) and QS-21 (0.02% w/v) in PBS at both 25 and 37 °C. Pristine P123 micelles and P123/QS-21 mixed formulations exhibited comparable D_h values (~20–21 nm) and very low PDI (<0.08) at both temperatures (Table 1 and Fig. 2a, b), indicating preservation of nanoscale organization upon QS-21 incorporation. The minimal temperature-dependent variation suggests a thermodynamically stable micellar population.

In contrast, pristine F127 PMs displayed larger D_h values (~37 nm at 25 °C), elevated PDI, and detectable unimeric populations (Table 1). Increasing the temperature to 37 °C resulted in partial micellar contraction (~26 nm) and moderate reduction in dispersity. Incorporation of QS-21 reduced average particle size and eliminated detectable unimers; however, PDI values remained higher than in P123-based systems, indicating greater structural heterogeneity.

Free QS-21 dispersions formed large and heterogeneous aggregates (D_h ≈ 316 nm; PDI ≈ 0.5), with broad size distributions that persisted at 37 °C (Table 1 and Fig. 2c, d), consistent with the known tendency of amphiphilic saponins to self-associate in aqueous media.[48] Importantly, such heterogeneous assemblies were not detected in mixed PMs, indicating that cooperative interaction with the copolymer matrix is

Table 1 Hydrodynamic diameter (D_h), size distribution, and polydispersity index (PDI) of pristine P123 and F127 PMs (2.5% w/v), P123/QS-21 and F127/QS-21 mixed PMs (2.5/0.02% w/v), and free QS-21 (0.02% w/v) in PBS at 25 and 37 °C, as determined by DLS. Values are reported as mean ± S.D. from three independent preparations ($n = 3$), with six DLS runs recorded per sample

		Peak		
Formulation	T [°C]	D_h [nm] (±S.D.)	% Intensity (±S.D.)	PDI (±S.D.)
P123	25	20.3 (0.9)	100.0 (0.0)	0.079 (0.029)
	37	21.0 (0.9)	100.0 (0.0)	0.066 (0.065)
P123/QS-21	25	20.6 (0.7)	100.0 (0.0)	0.065 (0.019)
	37	20.3 (1.3)	100.0 (0.0)	0.067 (0.018)
F127	25	36.9 (6.8)	93.1 (3.3)	0.287 (0.049)
	37	25.7 (1.1)	100.0 (0.0)	0.205 (0.020)
F127/QS-21	25	32.2 (3.2)	100.0 (0.0)	0.254 (0.051)
	37	25.1 (0.7)	100.0 (0.0)	0.180 (0.040)
Free QS-21	25	315.8 (59.2)	100.0 (0.0)	0.524 (0.119)
	37	222.4 (103.7)	100.0 (0.0)	0.463 (0.129)

consistent with suppression of QS-21 self-aggregation and promotes the formation of well-defined nanoscale assemblies. Raw intensity autocorrelation functions (Fig. S1a–c) further support these observations.

Together, these results indicate that cooperative assembly with P123 preserves a compact, monomodal, and temperature-insensitive nanoscale organization, whereas F127-based systems display greater architectural variability, reflecting weaker supramolecular cohesion under the evaluated conditions.

3.1.2 Apparent CMC and dilution-driven stability. The apparent CMC values determined in PBS at 37 °C (Table 2) provide insight into assembly energetics. Free QS-21 exhibited an apparent CMC above 0.32% (w/v), consistent with its limited colloidal stability and formation of heterogeneous aggregates (Table 1). Pristine P123 PMs displayed a low apparent CMC (~0.012% w/v), indicative of efficient micellization.

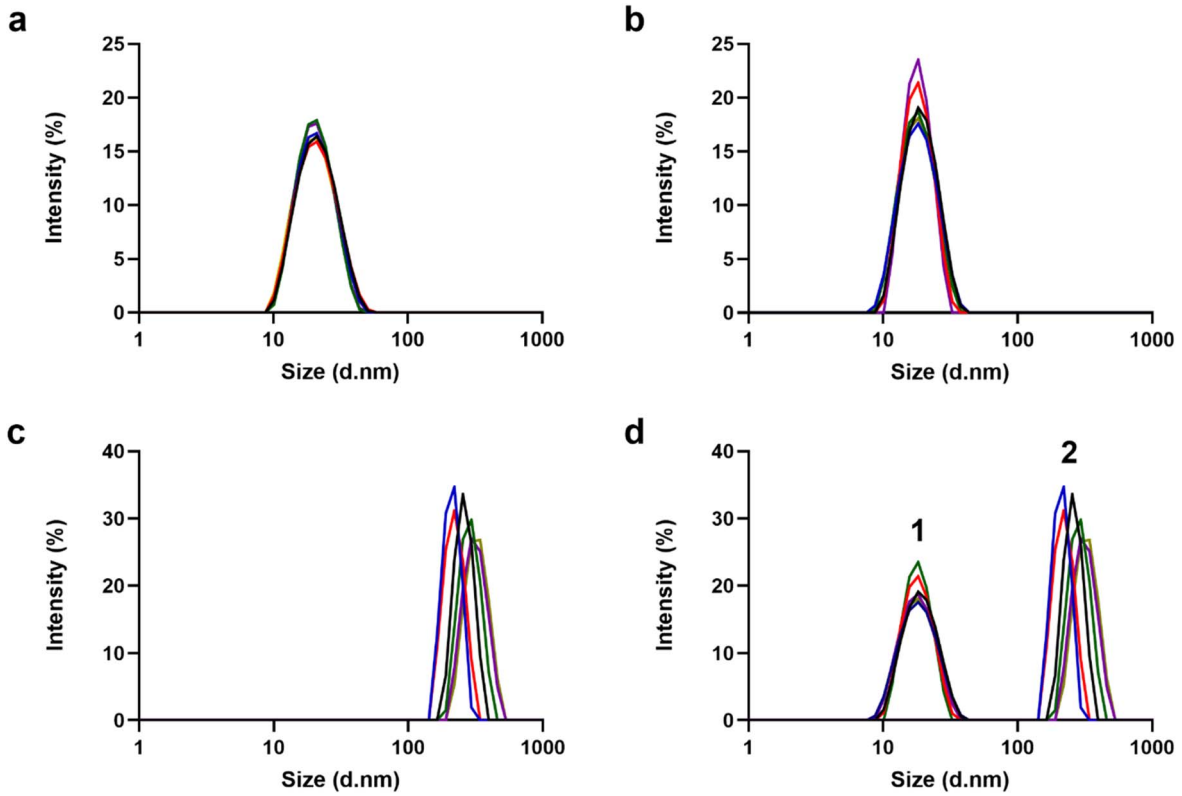

Fig. 2 DLS intensity-weighted size distributions of formulations dispersed in PBS and measured at 37 °C: (a) P123 PMs (2.5% w/v), (b) P123/QS-21 mixed PMs (2.5/0.02% w/v), (c) free QS-21 (0.02% w/v), and (d) overlaid distributions of P123/QS-21 mixed PMs (1) and free QS-21 (2). Data are representative of three independently prepared samples, each measured in six consecutive DLS runs.

Table 2 Experimental apparent critical micelle concentration (CMC) values of pristine P123 and F127 PMs, P123/QS-21 and F127/QS-21 mixed PMs, and free QS-21 in PBS at 37 °C, as determined by DLS, from changes in scattering intensity

Formulation	CMC (% w/v) PBS 37 °C
P123	0.012
P123/QS-21	0.016
F127	0.270
F127/QS-21	0.140
Free QS-21	$\gg$0.320

Incorporation of QS-21 resulted in only a slight increase (~0.016% w/v), maintaining a low threshold for assembly.

In contrast, pristine F127 PMs exhibited a substantially higher apparent CMC (~0.27% w/v). Although QS-21 incorporation reduced this value approximately twofold (~0.14% w/v), it remained significantly higher than that observed for P123/QS-21 (Table 2 and Fig. S2). These differences reflect intrinsic architectural effects. The lower HLB and reduced corona hydration of P123 likely promote tighter interfacial packing and enhanced micellization efficiency. Cooperative assembly is likely driven by hydrophobic anchoring of the QS-21 acyl chain within the PPO-rich micellar domains, combined with entropic stabilization arising from hydration of the exposed oligosaccharide moieties within the PEO corona. Thus, assembly appears to be governed by a balance between hydrophobic anchoring, interfacial packing, and corona-mediated steric stabilization rather than by a single dominant interaction. While apparent CMC values capture dilution stability, micellar architecture and interfacial packing emerge as the primary determinants of cooperative QS-21 incorporation.

In this context, simple partitioning would imply that QS-21 distributes between aqueous and micellar domains without significantly altering the thermodynamics of micelle formation. However, the observed shifts in apparent CMC, together with the pronounced differences in dilution stability between P123- and F127-based systems, suggest that QS-21 may influence the assembly process rather than solely redistributing within preformed micellar domains.

Stoichiometrically, QS-21 was present in molar minority relative to copolymer chains (approximately 43 : 1 P123 : QS-21 *versus* 20 : 1 F127 : QS-21). The higher molar excess and intrinsically lower apparent CMC of P123 favor efficient cooperative

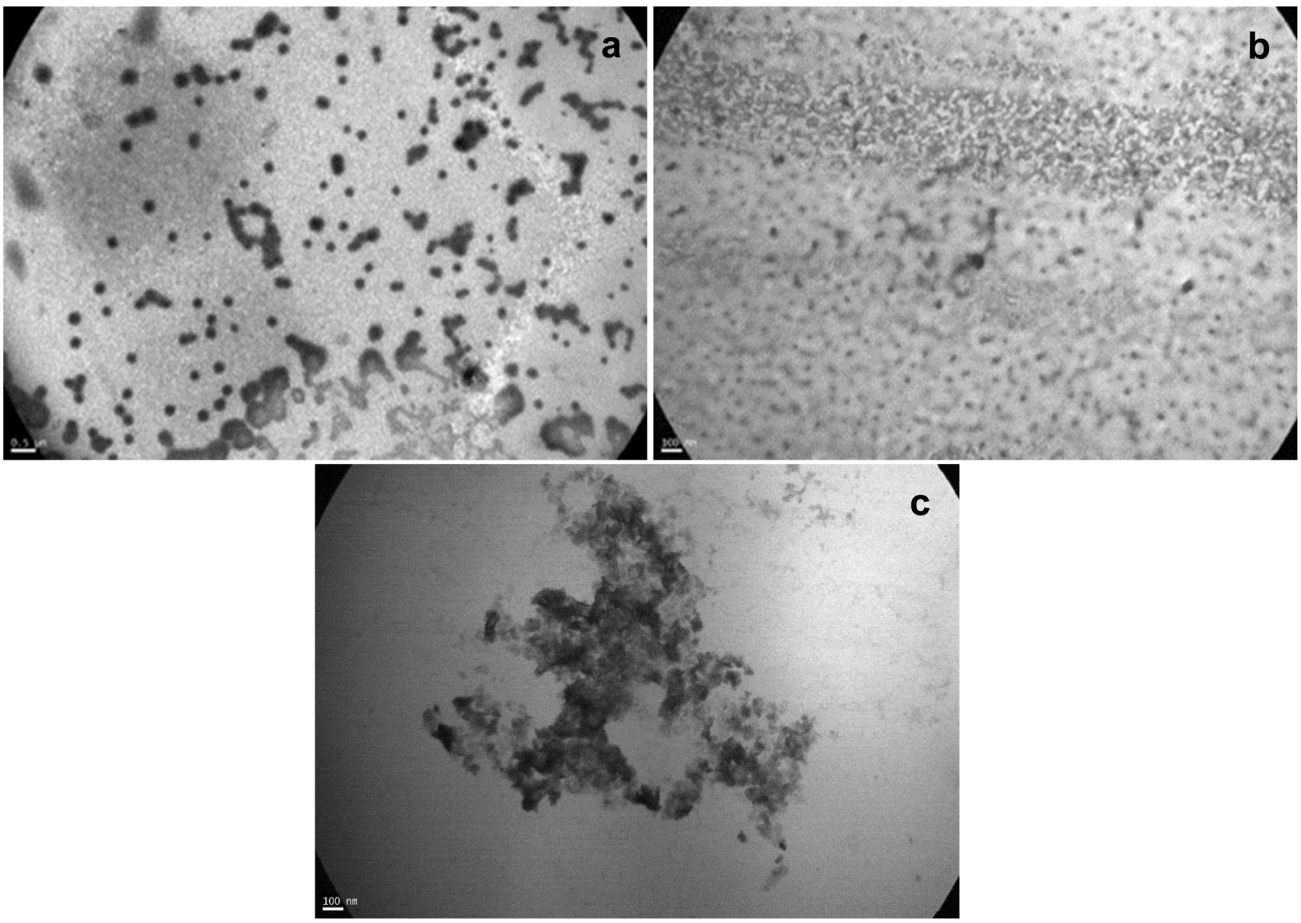

Fig. 3 Representative transmission electron microscopy (TEM) micrographs of (a) P123 PMs (2.5% w/v; scale bar: 500 nm), (b) P123/QS-21 mixed PMs (2.5/0.02% w/v; scale bar: 100 nm), and (c) free QS-21 (0.02% w/v; scale bar: 100 nm). Samples were pre-equilibrated at 37 °C for at least 1 h prior to imaging. Images are representative of multiple fields of view.

Table 3 Hydrodynamic diameter (D_h), particle concentration (particles mL^{-1}), and zeta potential of pristine P123 and F127 PMs, as well as P123/QS-21 and F127/QS-21 mixed PMs, measured in PBS at 25 °C by NTA. All formulations were prepared at high copolymer concentration (10% w/v) and subsequently diluted as indicated to enable single-particle tracking close to their apparent CMC

Formulation	D_h (nm) (±S.D.)	Particle concentration mL^{-1}	Dilution factor	Zeta potential (mV) (±S.D.)
P123	112.0 (43.2)	9.3×10^{11}	1/10 000	−31.5 (0.7)
P123/QS-21	117.4 (45.1)	1.3×10^{12}	1/10 000	−19.7 (1.5)
F127	156.6 (62.6)	3.3×10^{9}	1/100	−25.3 (1.0)
F127/QS-21	159.6 (75.9)	2.2×10^{9}	1/100	−17.1 (0.5)

accommodation of QS-21 within compact and dilution-resistant micelles.

Consistent with D_h analysis, P123/QS-21 maintained stable nanoscale populations at substantially lower copolymer concentrations than F127/QS-21, highlighting the critical role of copolymer architecture in dilution stability. Beyond dilution stability, these results indicate that cooperative supramolecular integration is consistent with a thermodynamically favorable reorganization, in which QS-21 contributes to micellar stabilization rather than solely residing within a pre-formed carrier. The distinct apparent CMC profiles observed for P123- and F127-based systems therefore reflect architecture-dependent differences in interfacial packing and energetic cooperativity, establishing polymer composition as a key determinant of nanoscale assembly robustness.

3.1.3 Micellar morphology, particle identity, and interfacial properties. TEM analysis revealed well-defined spherical nanostructures for P123 and P123/QS-21 (Fig. 3a and b), whereas free QS-21 displayed irregular aggregates (Fig. 3c), confirming effective structural integration upon cooperative assembly.

To probe the persistence of nanoscale assemblies under stringent dilution and near-threshold conditions, NTA was employed to quantify particle concentration and size distributions (Table 3). All formulations were initially prepared at high copolymer concentrations (10% w/v) to ensure complete micellar assembly while maintaining a fixed copolymer/QS-21 mass ratio (10/0.08% w/v), equivalent to the 2.5/0.02% (w/v) condition used for DLS and TEM. Samples were then diluted to concentrations close to their respective apparent CMC values. Under these conditions, P123-based systems remained readily detectable at dilution factors as high as 1/10 000, whereas F127-based systems required substantially lower dilution factors (~1/100) to achieve reliable particle tracking, reflecting a lower effective number density of persistent nanoscale entities (Table 3). While particle sizes measured by NTA were systematically larger (112–117 nm for P123 and P123/QS-21 and 157–160 nm for F127 and F127/QS-21) than D_h values obtained by DLS, as expected from the distinct physical principles of the techniques, NTA preserved the qualitative trends observed by DLS, with P123-based systems exhibiting smaller and more homogeneous particle populations relative to F127-based formulations (Table 3 and Fig. S3). Representative NTA videos (SI Videos S1 and S2) qualitatively support these differences, revealing faster Brownian motion and higher effective particle number densities for P123/QS-21 compared with F127/QS-21 under comparable tracking conditions.

Zeta potential measurements revealed moderately negative surface charges for all formulations (−32 to −20 mV for P123 and P123/QS-21 and −25 to −17 mV for F127 and F127/QS-21) (Table 3). QS-21 incorporation produced a reproducible decrease in the absolute zeta potential without inversion, consistent with interfacial reorganization of the mixed micelles rather than complete shielding. Together, DLS, apparent CMC, TEM, and NTA analyses converge to identify P123/QS-21 as the most structurally coherent among the systems evaluated. Importantly, this structural coherence emerges from architecture-dependent supramolecular integration rather than passive confinement, underscoring that nanoscale stability is an intrinsic consequence of copolymer–saponin cooperativity.

3.1.4 Microenvironmental fluorescence probing and comparative analysis. Fluorescein free acid in PBS (0.5 μM) exhibited stable fluorescence at neutral pH, with no significant temperature dependence. In the presence of PEO–PPO PMs, a decrease in fluorescence intensity was observed at both room temperature and 37 °C, consistent with the presence of micellar assemblies and modification of the probe microenvironment (Fig. 4a). P123 and F127 produced comparable reductions, indicating similar probe environments under these conditions.

Upon incorporation of QS-21, a concentration-dependent decrease in fluorescence intensity was observed in both systems (Fig. 4b), more pronounced in P123-based formulations. Notably, a statistically significant reduction was observed above 0.32% (w/v) QS-21, indicating a marked change in the probe environment.

Comparison with theoretical additive responses reveals systematic deviations from the additive model across the explored concentration range (Fig. S4), indicating that the experimental behavior cannot be reconstructed from the independent contributions of QS-21 and the copolymer.

The decrease in fluorescence intensity is consistent with changes in local polarity, molecular mobility, and probe accessibility. Taken together, these observations suggest that QS-21 incorporation is associated with modifications in the local microenvironment beyond those expected from simple redistribution within pre-existing micellar domains.

3.2 Regulation of QS-21 membrane activity

QS-21 is intrinsically hemolytic due to its interaction with cholesterol-rich membranes.[43,57] Pristine P123 and F127 exhibited negligible hemolytic activity (<5%), confirming that the copolymers themselves do not disrupt membranes (Fig. 5a).

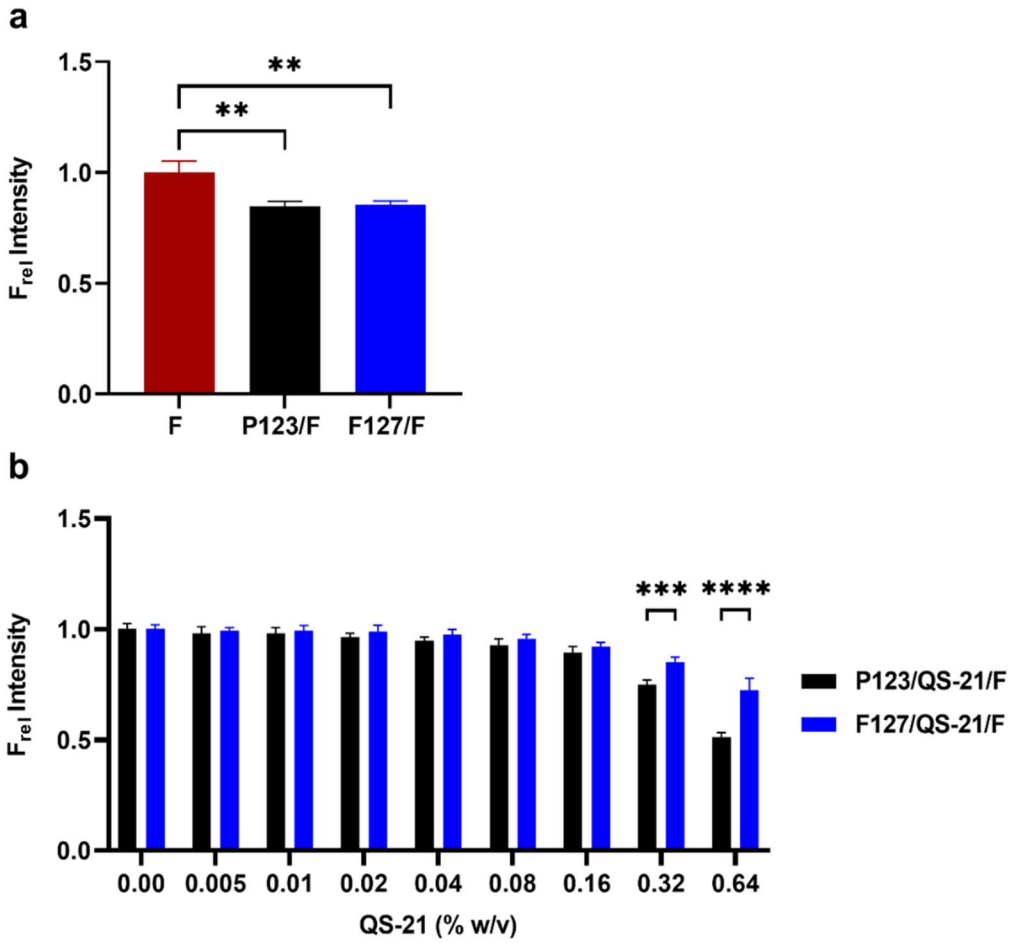

Fig. 4 Relative fluorescence intensity (F_{rel} intensity) of free fluorescein (F) and F in single and mixed polymeric micelles (PMs): (a) P123/F and F127/F PMs (2.5% w/v/0.5 μM), where F_{rel} intensity is expressed relative to free F (0.5 μM) in PBS. (b) P123/QS-21/F and F127/QS-21/F mixed PMs (2.5% w/v copolymer, 0.005–0.64% w/v QS-21 and 0.5 μM F) in PBS, where F_{rel} intensity is expressed relative to the corresponding copolymer–F formulations (P123/F or F127/F, 2.5% w/v/0.5 μM). Samples were incubated at 37 °C for 30 min prior to measurement. Excitation and emission wavelengths were set at 455 and 515 nm, respectively. Measurements were performed using a gain of 85 and 15 flashes per point, after subtraction of the corresponding blank. Data are presented as mean ± S.D. ($n = 3$). Statistical analysis was performed using (a) one-way ANOVA and (b) two-way ANOVA, followed by Bonferroni's multiple comparison test. In panel (a), statistical comparisons were made relative to free F. In panel (b), statistical comparisons correspond to differences between P123/QS-21/F and F127/QS-21/F at each QS-21 concentration. Statistical significance is indicated as $^{**}p < 0.01$, $^{***}p < 0.001$, and $^{****}p < 0.0001$.

Incorporation of QS-21 into P123 PMs resulted in concentration-dependent attenuation of hemolysis relative to free QS-21, with reductions up to ~20% at ≥0.02% (w/v) (Fig. 5b). Importantly, hemolysis was not completely suppressed, indicating that QS-21 remains partially accessible at the micellar interface rather than fully sequestered. Partial anchoring of the QS-21 acyl chain within the micellar hydrophobic domains may contribute to stabilization of the saponin within the supramolecular assembly while preserving interfacial accessibility of its bioactive motifs, a feature that may be essential for maintaining immunostimulatory function.

F127/QS-21 formulations showed only modest attenuation (~14% at 0.16% w/v; Fig. S5), reinforcing that this is consistent with a role of cooperative organization in regulating QS-21 membrane activity. Attenuation of hemolysis is not consistent with complete sequestration of QS-21, but rather with reduced cooperative interaction density at the membrane interface, resulting from controlled interfacial presentation. Micellar incorporation appears to modulate QS-21 membrane activity, potentially through redistribution of interfacial presentation across a polymeric interface, thereby lowering local disruptive events while preserving immunostimulatory accessibility.

Together, these findings are consistent with a supramolecular modulation framework in which copolymer architecture may influence the dynamic interfacial presentation of QS-21. Notably, the PEO–PPO copolymers used here have a well-established safety profile with low cytotoxicity reported across multiple cell types;[23–26,31] however, incorporation of QS-21 gives rise to a new supramolecular entity that warrants dedicated biological evaluation. Although the attenuation of hemolytic activity is moderate (~20%), this effect should be interpreted in the context of the intrinsically strong membrane activity of QS-21. Within this framework, hemolysis serves as a stringent comparative indicator of membrane interaction rather than

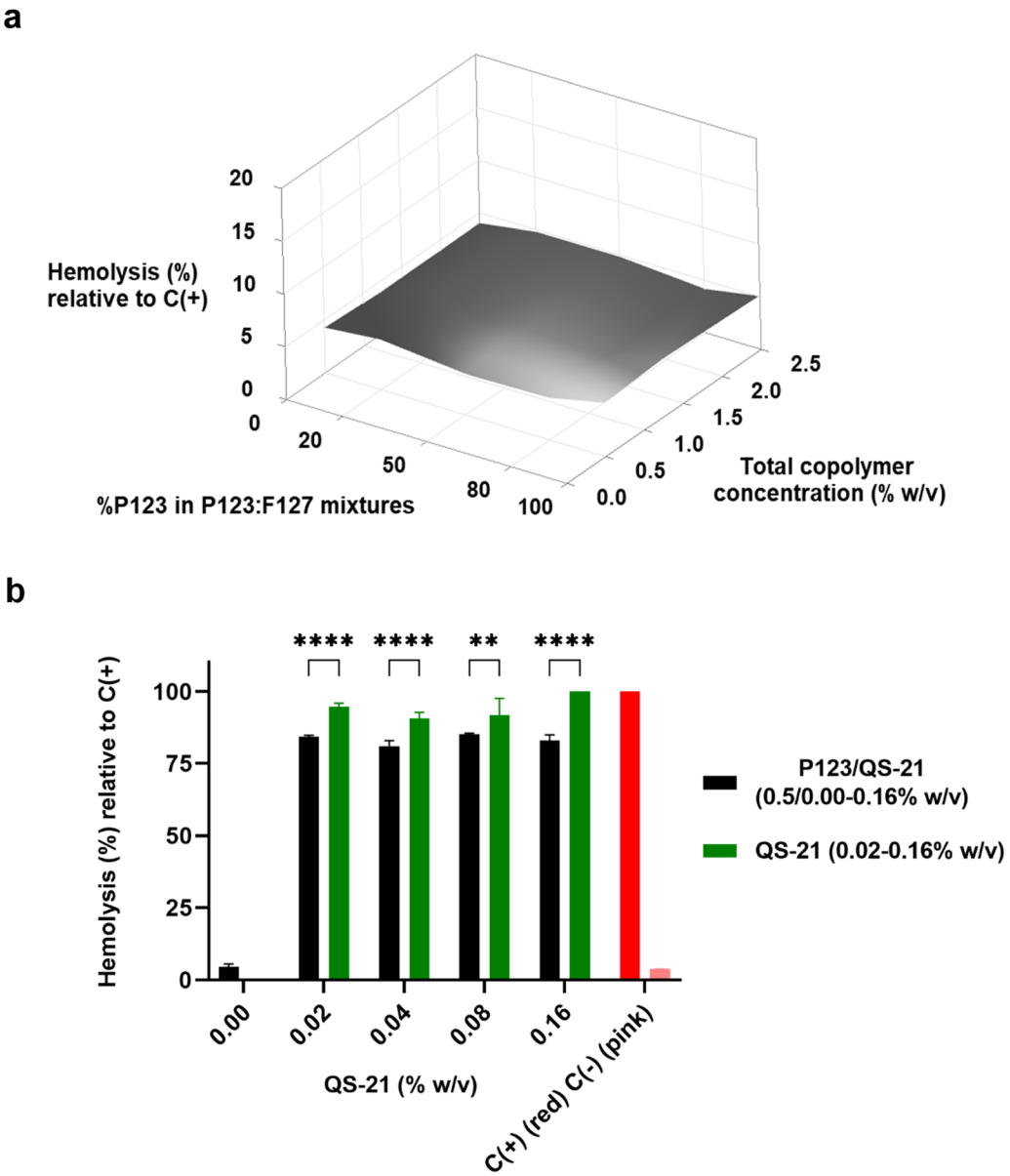

Fig. 5 Evaluation of the hemolytic behavior of P123 and F127 PMs, P123/F127 mixed PMs, and free QS-21. (a) Three-dimensional surface plot showing hemolysis (%) relative to the positive control C(+) as a function of the P123 percentage in P123 : F127 mixtures and the total copolymer concentration (% w/v). Free QS-21 (0.16% w/v; $n = 6$) was used as C(+), and a 5% red blood cell suspension ($n = 6$) served as the negative control C(−). (b) Hemolysis (%) relative to C(+) for P123 PMs, P123/QS-21 mixed PMs, and free QS-21. QS-21 was evaluated over the concentration range 0.02–0.16% (w/v). A reduction in hemolysis was observed for P123/QS-21 mixed PMs compared to free QS-21 at equivalent QS-21 concentrations. Data are presented as mean ± S.D. ($n = 3$). Statistical analysis was performed using two-way ANOVA followed by Bonferroni's multiple comparison test. In panel (b), statistical comparisons correspond to differences between P123/QS-21 and free QS-21 at each concentration. Statistical significance is indicated as $^{**}p < 0.01$ and $^{****}p < 0.0001$.

a direct predictor of *in vivo* safety, consistent with the absence of observable adverse effects under the conditions tested. Rather than completely shielding the saponin, cooperative integration attenuates hemotoxicity while preserving partial membrane accessibility likely required for immunostimulatory activity. This architecture-dependent regulation underscores the importance of interfacial organization as a controllable biomaterials parameter for tuning the balance between safety and biological function.

3.3 Antigen compatibility and nanoscale integrity

Spike protein alone formed large and heterogeneous aggregates in the 300–500 nm range in PBS (Table 4 and Fig. 6a, b), consistent with the tendency of recombinant proteins to form higher-order assemblies under physiological ionic strength. In contrast, P123/QS-21/Spike preserved a dominant micellar population (~20–23 nm), together with minor larger protein-associated species (Table 4 and Fig. 6c, d). Autocorrelation

Table 4 Hydrodynamic diameter (D_h), size distribution, and polydispersity index (PDI) of P123/QS-21 (adjuvant control, 2.5/0.02% w/v), Spike PBS (antigen control, 0.07 mg mL^{-1}), and P123/QS-21/Spike formulations in PBS at 25 and 37 °C, as determined by DLS. Values are reported as mean ± S.D. from three independent preparations ($n = 3$), with six DLS runs recorded per sample[a]

		Peak 1		Peak 2		
Formulation	T [°C]	D_h [nm] (±S.D.)	% Intensity (±S.D.)	D_h [nm] (±S.D.)	% Intensity (±S.D.)	PDI (±S.D.)
P123/QS-21	25	20.6 (0.7)	100.0 (0.0)	—	—	0.065 (0.019)
	37	20.3 (1.3)	100.0 (0.0)	—	—	0.067 (0.018)
Spike PBS	25	441.4 (135.4)	75.2 (6.8)	92.2 (30.4)	24.8 (6.8)	0.514 (0.068)
	37	344.2 (106.4)	100.0 (0.0)	—	—	0.375 (0.057)
P123/QS-21/Spike	25	23.5 (1.4)	71.2 (12.3)	523.5 (173.5)	28.8 (12.3)	0.457 (0.170)
	37	23.2 (0.7)	72.4 (11.6)	464.9 (115.4)	27.6 (11.6)	0.453 (0.160)

[a] Peak 1 corresponds to the main nanoscale population, while peak 2 represents a minor population associated with Spike-derived species. "—" indicates that no secondary population was detected under the experimental conditions.

functions confirmed stable nanoscale organization despite the coexistence of minor larger scattering entities (Fig. 6d).

Importantly, the presence of Spike protein did not induce detectable micellar destabilization or broadening of the dominant nanoscale population, suggesting that the cooperative supramolecular architecture of P123/QS-21 micelles remains structurally stable in the presence of antigen. This observation suggests that Spike molecules likely interact with the micellar system primarily through interfacial association rather than disruptive penetration or aggregation-induced destabilization.

The preservation of a narrow micellar size distribution further indicates that antigen incorporation occurs without perturbing the underlying polymer–saponin organization established during cooperative self-assembly. Such behavior is consistent with colloidal compatibility between the antigen and the micellar interface, enabling the coexistence of nanoscale

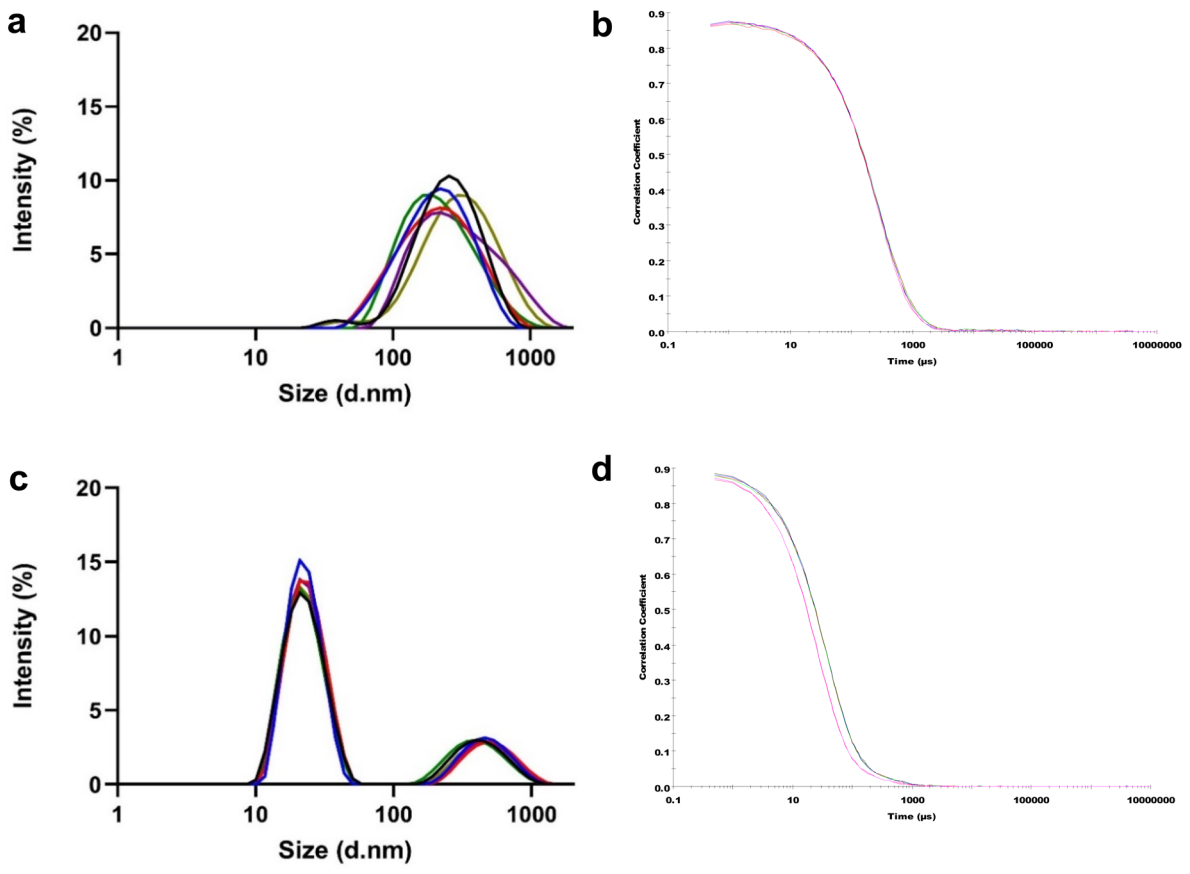

Fig. 6 Hydrodynamic size characterization of Spike protein-based formulations in PBS at 37 °C by DLS. (a and c) Intensity-weighted size distributions as a function of particle diameter (nm) for free Spike protein (0.07 mg mL^{-1}) (a) and P123/QS-21/Spike mixed PMs (2.5/0.02% w/v) (c). (b and d) Corresponding intensity autocorrelation functions. Data are representative of three independently prepared samples, each measured in six consecutive DLS runs.

micelles and protein-associated species within the same formulation environment.

From a formulation perspective, these findings suggest that antigen incorporation can be achieved without requiring covalent conjugation, encapsulation strategies, or structural modification of the antigen. The ability of P123/QS-21 micelles to maintain nanoscale integrity in the presence of Spike protein therefore supports a simplified co-formulation strategy in which antigen and nanoadjuvant coexist within a single supramolecular system while preserving their structural and functional identities.

3.4 *In vivo* adjuvant performance and functional neutralization

Immunization with P123/QS-21/Spike induced approximately a twofold increase in anti-Spike antibody responses in serum relative to Spike PBS (Fig. 7a). In BAL, responses were enhanced by approximately one order of magnitude (Fig. 7b), indicating robust mucosal immunity in the respiratory tract. Neutralizing

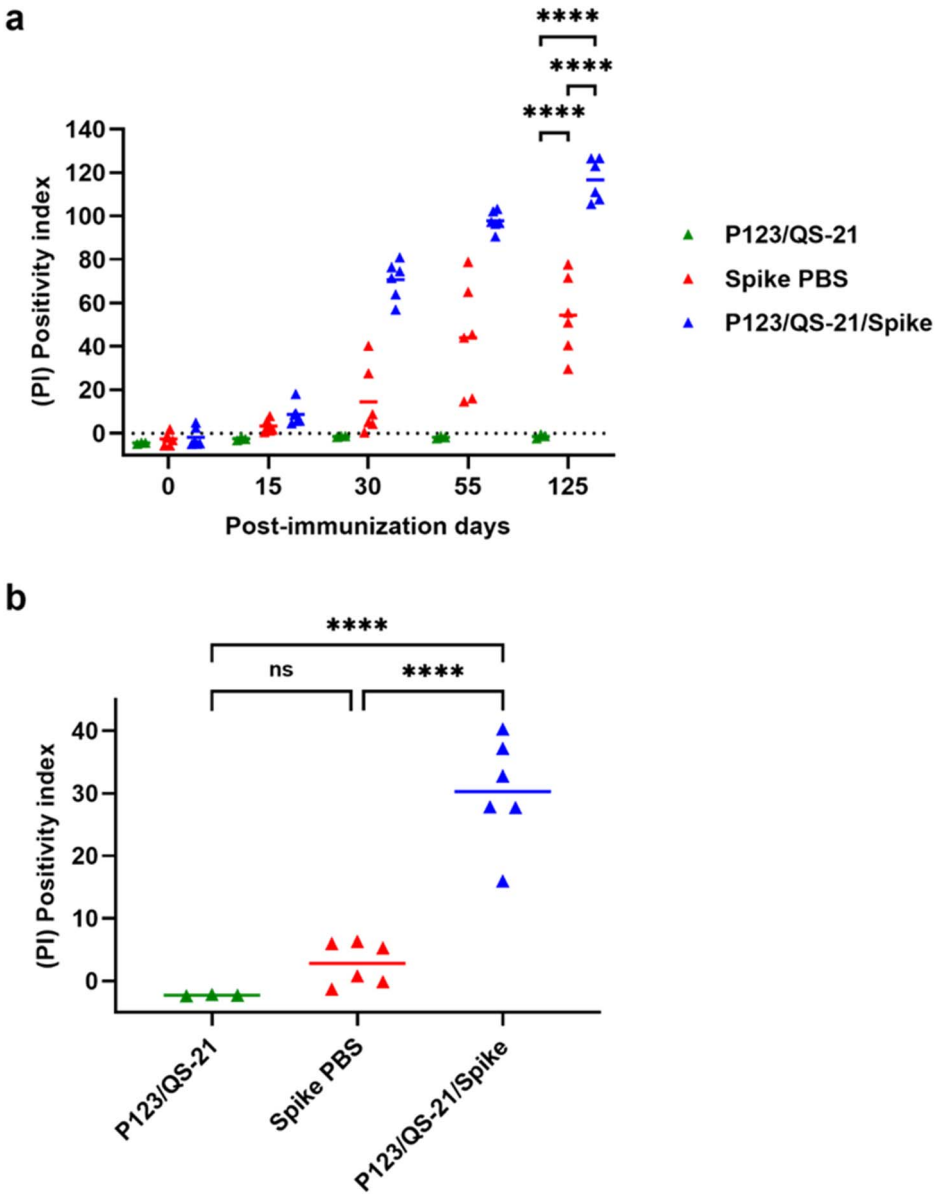

Fig. 7 *In vivo* immune response elicited by P123/QS-21 mixed PMs and Spike-based formulations across the different experimental groups. Positivity index (PI) of anti-Spike antibodies measured in (a) serum during the immunization schedule and (b) bronchoalveolar lavage (BAL) after protocol completion. At day 125 post-immunization, the P123/QS-21/Spike formulation elicited higher systemic and mucosal anti-Spike responses than control groups (P123/QS-21 without antigen and Spike in PBS). No significant differences were observed between control groups in BAL. Data are presented as mean ± S.D. Statistical analysis was performed using (a) two-way ANOVA and (b) one-way ANOVA, followed by Bonferroni's multiple comparison test. Statistical comparisons correspond to differences between experimental groups as indicated by the figure annotations. Statistical significance is indicated as ns (not significant) and ****$p < 0.0001$.

Table 5 Neutralizing activity and anti-Spike antibody response following the immunization protocol. Neutralizing activity is reported qualitatively (+/−) and quantitatively as neutralizing titers measured after the third dose. Anti-Spike antibody levels in serum and BAL are expressed as positivity index (PI) at the final bleed. Dashes (−) indicate absence of detectable neutralizing activity or titers below the limit of detection. Positive controls included hyperimmune equine serum (HES) and vaccinated human serum (VHS)

Treatment	Animal ID	Neutralizing activity	Neutralizing titer (post 3rd dose)	Final bleed	
				Serum PI	BAL PI
P123/QS-21	25	−	−	−1.19	14.85
	26	−	−	−2.17	−2.13
	27	−	−	−0.49	−2.34
Spike PBS	28	+	<8	55.55	0.83
	29	+	32	29.72	−0.10
	30	−	−	77.82	6.33
	31	+	<8	51.01	5.32
	32	+	<8	71.66	5.98
	33	−	−	40.62	−1.29
P123/QS-21/Spike	34	−	−	111.02	27.89
	35	+	>1024	126.56	27.75
	36	+	64	107.66	40.31
	37	−	−	123.05	32.82
	38	+	512	105.56	15.99
	39	+	512	126.64	37.22
Positive control	HES	+	>1024	−	−
	VHS	+	512	−	−

antibodies were detected exclusively in animals receiving P123/QS-21/Spike (Table 5), demonstrating that enhanced humoral magnitude translated into functional inhibition of the ACE2–RBD interaction. These results provide functional support for the proposed supramolecular design principle, demonstrating that architecture-controlled interfacial presentation of QS-21 is consistent with the enhanced immunological output observed *in vivo*.

Collectively, these results support the concept that controlled interfacial presentation of QS-21 within P123-based micelles preserves immunostimulatory accessibility while mitigating excessive membrane disruption, enabling a favorable balance between safety and functional potency *in vivo*. The dimensions of P123/QS-21 assemblies (~21 nm) fall within a size range generally associated with uptake by APCs and lymphatic drainage, facilitating antigen transport to lymph nodes where adaptive responses are initiated.[9,59,63] Thus, nanoscale organization achieved through cooperative assembly appears to be both structurally and biologically relevant.

Together, these observations support a structure–interfacial activity–immune response relationship, in which cooperative nanoscale organization may influence QS-21 bioavailability at immune-relevant interfaces. Enhanced mucosal and systemic responses emerge as a downstream consequence of controlled supramolecular organization, rather than arising solely from independent formulation effects.

The adjuvant-only control group (P123/QS-21, $n = 3$) was included as an exploratory reference; while this may limit statistical power for this specific comparison, the overall conclusions are supported by larger experimental groups and consistent trends across independent immunological readouts.

Within this framework, it is also important to note that the present study was designed as a controlled system to establish structure–function relationships within polymeric micellar platforms. Accordingly, direct comparison with clinically benchmarked adjuvants (*e.g.*, AS01 or Alhydrogel-based formulations) was not included here, but will be important to further contextualize the translational relevance of the observed responses.

3.5 Supramolecular implications and translational context

QS-21 is incorporated into multiple licensed and clinical-stage platforms, including AS01, AS02, AS05, AS015, and ISCOM-based systems.[43–47,49–52,64–66] While highly effective, these platforms largely rely on lipid-based assemblies and cholesterol-mediated stabilization strategies, which may introduce scale-sensitive manufacturing constraints.[67,68] In this context, the present platform explores polymer-driven cooperative supramolecular organization as an alternative means to modulate QS-21 activity through architecture-dependent interfacial positioning within PEO–PPO micelles.

QS-21 appears to contribute to the supramolecular organization of the micelles, linking polymer architecture to interfacial membrane activity and downstream immune responses.

Comparative analysis of P123- and F127-based systems demonstrates that nanoscale organization correlates with dilution stability, membrane modulation, and emergent immune responses, supporting a structure–interfacial activity–immune function relationship and highlighting cooperative molecular integration as a promising biomaterials design strategy for tunable nanoadjuvants.

Beyond hemolytic modulation, QS-21 is known to undergo pH- and temperature-dependent hydrolytic degradation of its ester functionalities in aqueous environments.[48,57,58] No detectable hydrolysis of QS-21 was observed either in free solution or

within the micellar formulations under the experimental conditions employed. Although detailed stability studies were beyond the scope of the present work, cooperative integration within PPO-rich micellar domains may also influence the interfacial exposure of hydrolytically sensitive motifs, a positioning that may be particularly relevant under physiological formulation conditions where preservation of adjuvant integrity is required for consistent immunological performance.

Collectively, these findings support a perspective in which QS-21 formulation can be approached not only through stabilization strategies but also through controlled supramolecular organization which may contribute to biological activity. Ongoing studies are aimed at further elucidating the molecular basis of copolymer–saponin cooperativity using complementary spectroscopic and kinetic approaches. Together, these results support cooperative self-assembly as a rational and potentially transferable strategy to improve the safety, performance, and manufacturability of QS-21-based subunit vaccine adjuvants.

4. Conclusions and perspectives

This work shows that QS-21 can be incorporated into PEO–PPO PMs through cooperative assembly, generating structurally coherent mixed PMs in which the saponin appears to participate in the supramolecular organization of the assemblies. By systematically comparing P123 and F127 architectures, we show that copolymer composition influences nanoscale organization, dilution stability, and interfacial behavior.

Among the systems evaluated, P123/QS-21 assemblies exhibited superior structural robustness, monodispersity, and resistance to dilution, together with controlled attenuation of hemolytic activity. Importantly, this architecture-dependent modulation of membrane interaction preserved immunostimulatory function and was associated with enhanced systemic and mucosal anti-Spike responses, as well as functional neutralizing antibodies *in vivo*. These findings suggest a connection between supramolecular organization and biological performance.

In contrast to strategies based on partial or complete stabilization of QS-21 within cholesterol-rich assemblies, this strategy introduces cooperative integration as a controllable interface-engineering approach for membrane-active immunomodulators. Cooperative organization may therefore emerge not merely as a structural feature, but as a factor contributing to adjuvant safety and potency.

Given the thermoresponsive nature of PEO–PPO copolymers at higher concentrations, future studies may explore transitions between lymphatic-draining nanoadjuvants and in situ-forming depot systems, enabling additional spatiotemporal control over antigen–adjuvant presentation.[9,25,69]

Collectively, these results support copolymer–saponin mixed micelles as a scalable and versatile nanoadjuvant platform compatible with simplified co-formulation strategies and adaptable manufacturing routes. Beyond QS-21, this cooperative supramolecular framework may be extended to other amphiphilic immunomodulators whose biological activity depends on interfacial presentation, providing a conceptual and translational basis for the development of next-generation subunit vaccine adjuvants.

Author contributions

Conceptualization, P. G. M., F. J. W. and R. J. G.; methodology, P. G. M., F. J. W. and R. J. G.; software, P. G. M., L. G. A., J. I. M., A. C. M., S. N. V., F. J. W. and R. J. G.; validation, P. G. M., F. J. W. and R. J. G.; formal analysis, P. G. M., L. G. A., J. I. M., A. C. M., S. N. V., M. V. M., F. J. W. and R. J. G.; investigation, P. G. M., L. G. A., J. I. M., A. C. M., M. L. F., S. N. V., F. J. W. and R. J. G.; resources, I. S., M. V. M., F. J. W. and R. J. G.; data curation, P. G. M. and R. J. G.; writing-original draft, P. G. M., F. J. W. and R. J. G.; writing-review & editing, P. G. M., L. G. A., M. L. F., S. N. V., M. V. M., F. J. W. and R. J. G.; supervision, F. J. W. and R. J. G.; project administration, F. J. W. and R. J. G.; funding acquisition, F. J. W. and R. J. G. All authors have read and agreed to the published version of the manuscript.

Conflicts of interest

There are no conflicts to declare regarding the publication of this article.

Data availability

Data for this article are available at Repositorio Institucional CONICET Digital https://datosdeinvestigacion.conicet.gov.ar/. Complete data are available from the corresponding author upon reasonable request.

Supplementary information (SI): additional physicochemical characterization (DLS autocorrelation functions, derived count rate profiles and apparent CMC determination), nanoparticle tracking analysis (NTA), microenvironmental fluorescence assays, hemolysis studies, and representative NTA video recordings supporting the main findings of this study. See DOI: https://doi.org/10.1039/d6ra01909a.

Acknowledgements

P. G. M. gratefully acknowledges the Consejo Nacional de Investigaciones Científicas y Técnicas (CONICET) for his doctoral fellowship. I. S. is a member of the University of Buenos Aires. L. G. A., J. I. M., A. C. M., M. L. F., M. V. M., S. N. V., F. J. W. and R. J. G. are members of CONICET. The authors sincerely thank Trebe Biotech SRL (Pergamino, Buenos Aires, Argentina) for kindly providing the recombinant SARS-CoV-2 Spike antigen used in this study. The authors also thank Dr Marcela Cucher (IMPAM, UBA-CONICET) for her invaluable assistance with nanoparticle tracking analysis (NTA) measurements. This work was partially supported by CONICET, Universidad de Buenos Aires (UBA-CyT 20020170100128BA, 20020190200182BA and PreInc UBA 2025 Program), and Agencia Nacional de Promoción de la Investigación, el Desarrollo Tecnológico y la Innovación (PICT 2019-03331).

References

1 V. Kayser and I. Ramzan, Vaccines and vaccination: history and emerging issues, *Hum. Vaccines Immunother.*, 2021, **17**, 5255–5268, DOI: 10.1080/21645515.2021.1977057.
2 A. Kocourkova, J. Honegr, K. Kuca and J. Danova, Vaccine Ingredients: Components that Influence Vaccine Efficacy, *Mini-Rev. Med. Chem.*, 2017, **17**, 451–466, DOI: 10.2174/1389557516666160801103303.
3 I. Delany, R. Rappuoli and E. De Gregorio, Vaccines for the 21st century, *EMBO Mol. Med.*, 2014, **6**, 708–720, DOI: 10.1002/emmm.201403876.
4 P. M. Moyle, Progress in vaccine development, *Curr. Protoc. Microbiol.*, 2015, **36**, 18.1.1–18.1.26, DOI: 10.1002/9780471729259.mc1801s36.
5 Z. B. Wang and J. Xu, Better Adjuvants for Better Vaccines: Progress in Adjuvant Delivery Systems, Modifications, and Adjuvant–Antigen Codelivery, *Vaccines*, 2020, **8**, 128, DOI: 10.3390/vaccines8010128.
6 A. Bouazzaoui, A. A. H. Abdellatif, F. A. Al-Allaf, N. M. Bogari, S. Al-Dehlawi and S. H. Qari, Strategies for Vaccination: Conventional Vaccine Approaches Versus New-Generation Strategies in Combination with Adjuvants, *Pharmaceutics*, 2021, **13**, 140, DOI: 10.3390/pharmaceutics13020140.
7 M. O. Oyewumi, A. Kumar and Z. Cui, Nano-microparticles as immune adjuvants: correlating particle sizes and the resultant immune responses, *Expert Rev. Vaccines*, 2010, **9**, 1095–1107, DOI: 10.1586/erv.10.89.
8 S. K. Verma, P. Mahajan, N. K. Singh, A. Gupta, R. Aggarwal, R. Rappuoli and A. K. Johri, New-age vaccine adjuvants, their development, and future perspective, *Front. Immunol.*, 2023, **14**, 1043109, DOI: 10.3389/fimmu.2023.1043109.
9 P. G. Márquez, F. J. Wolman and R. J. Glisoni, Nanotechnology platforms for antigen and immunostimulant delivery in vaccine formulations, *NanoTrends*, 2024, **8**, 100058, DOI: 10.1016/j.nwnano.2024.100058.
10 T. Zhao, Y. Cai, Y. Jiang, X. He, Y. Wei, Y. Yu and X. Tian, Vaccine adjuvants: mechanisms and platforms, *Signal Transduction Targeted Ther.*, 2023, **8**, 283, DOI: 10.1038/s41392-023-01557-7.
11 A. Kaur, J. Baldwin, D. Brar, D. B. Salunke and N. Petrovsky, Toll-like receptor (TLR) agonists as a driving force behind next-generation vaccine adjuvants and cancer therapeutics, *Curr. Opin. Chem. Biol.*, 2022, **70**, 102172, DOI: 10.1016/j.cbpa.2022.102172.
12 A. Garg and H. K. Dewangan, Nanoparticles as Adjuvants in Vaccine Delivery, *Crit. Rev. Ther. Drug Carrier Syst.*, 2020, **37**, 183–204, DOI: 10.1615/CritRevTherDrugCarrierSyst.2020033273.
13 U.S. Food and Drug Administration, *Vaccines Licensed for Use in the United States*, https://www.fda.gov/vaccines-blood-biologics/vaccines/vaccines-licensed-use-united-states, accessed Jan 6, 2026.
14 European Medicines Agency, *Medicines Authorised: Vaccines for Human Use*, https://www.ema.europa.eu, accessed Jan 6, 2026.
15 A. Facciolà, G. Visalli, P. Laganà, V. La Fauci, R. Squeri, G. F. Pellicanò, G. Nunnari, M. Trovato and A. Di Pietro, The new era of vaccines: the "nanovaccinology", *Eur. Rev. Med. Pharmacol. Sci.*, 2019, **23**, 7163–7182, DOI: 10.26355/eurrev_201908_18763.
16 A. Das and N. Ali, Nanovaccine: an emerging strategy, *Expert Rev. Vaccines*, 2021, **20**, 1273–1290, DOI: 10.1080/14760584.2021.1984890.
17 M. Kheirollahpour, M. Mehrabi, N. M. Dounighi, M. Mohammadi and A. Masoudi, Nanoparticles and Vaccine Development, *Pharm. Nanotechnol.*, 2020, **8**, 6–21, DOI: 10.2174/2211738507666191024162042.
18 D. Lozano, V. Larraga, M. Vallet-Regí and M. Manzano, An Overview of the Use of Nanoparticles in Vaccine Development, *Nanomaterials*, 2023, **13**, 1828, DOI: 10.3390/nano13121828.
19 B. Pulendran, P. S. Arunachalam and D. T. O'Hagan, Emerging concepts in the science of vaccine adjuvants, *Nat. Rev. Drug Discovery*, 2021, **20**, 454–475, DOI: 10.1038/s41573-021-00163-y.
20 E. H. Kim, M. C. Woodruff, L. Grigoryan, B. Maier, S. H. Lee, P. Mandal, M. Cortese, M. S. Natrajan, R. Ravindran, H. Ma, M. Merad, A. D. Gitlin, E. S. Mocarski, J. Jacob and B. Pulendran, Squalene emulsion-based vaccine adjuvants stimulate CD8 T cell but not antibody responses, through a RIPK3-dependent pathway, *eLife*, 2020, **9**, e52687, DOI: 10.7554/eLife.52687.
21 E. J. Ko and S. M. Kang, Immunology and efficacy of MF59-adjuvanted vaccines, *Hum. Vaccines Immunother.*, 2018, **14**, 3041–3045, DOI: 10.1080/21645515.2018.1495301.
22 A. Mendes, J. Azevedo-Silva and J. C. Fernandes, From Sharks to Yeasts: Squalene in the Development of Vaccine Adjuvants, *Pharmaceuticals*, 2022, **15**, 265, DOI: 10.3390/ph15030265.
23 N. Lecot, R. Glisoni, N. Oddone, J. Benech, M. Fernández, J. P. Gambini, P. Cabral and A. Sosnik, Glucosylated Polymeric Micelles Actively Target a Breast Cancer Model, *Adv. Ther.*, 2021, **4**, 2000010, DOI: 10.1002/adtp.202000010.
24 N. Lecot, B. Dávila, C. Sánchez, M. Fernández, M. González, P. Cabral, H. Cerecetto and R. Glisoni, Development and Evaluation of 2-Amino-7-Fluorophenazine 5,10-Dioxide Polymeric Micelles as Antitumoral Agents for 4T1 Breast Cancer, *Polymers*, 2022, **14**, 71, DOI: 10.3390/polym14010071.
25 N. Lecot, M. Fernández-Lomónaco, H. Cerecetto, J. P. Gambini, P. Cabral and R. Glisoni, Indocyanine green within glycosylated polymeric micelles as potential image agents to map sentinel lymph nodes and breast cancer, *RSC Pharm.*, 2024, **1**, 57–67, DOI: 10.1039/d3pm00053b.
26 R. Castelli, M. Ibarra, R. Faccio, I. Miraballes, M. Fernández, A. Moglioni, P. Cabral, H. Cerecetto, R. J. Glisoni and V. Calzada, T908 Polymeric Micelles Improved the Uptake of Sgc8-c Aptamer Probe in Tumor-Bearing Mice: A Co-Association Study between the Probe and Preformed

Nanostructures, *Pharmaceuticals*, 2022, **15**, 15, DOI: 10.3390/ph15010015.

27 R. J. Glisoni and A. Sosnik, Encapsulation of the antimicrobial and immunomodulator agent nitazoxanide within polymeric micelles, *J. Nanosci. Nanotechnol.*, 2014, **14**, 4670–4682, DOI: 10.1166/jnn.2014.8647.

28 M. L. Cuestas, R. J. Glisoni, V. L. Mathet and A. Sosnik, Lactosylated poly(ethylene oxide)–poly(propylene oxide) block copolymers for potential active targeting: synthesis and physicochemical and self-aggregation characterization, *J. Nanopart. Res.*, 2013, **15**, 1389, DOI: 10.1007/s11051-012-1389-0.

29 R. J. Glisoni and A. Sosnik, Novel poly(ethylene oxide)-co-poly(propylene oxide) copolymer-glucose conjugate by microwave-assisted ring opening of a sugar lactone, *Macromol. Biosci.*, 2014, **14**, 1639–1651, DOI: 10.1002/mabi.201400235.

30 C. Alvarez-Lorenzo, A. Sosnik and A. Concheiro, PEO-PPO block copolymers for passive micellar targeting and overcoming multidrug resistance in cancer therapy, *Curr. Drug Targets*, 2011, **12**, 1112–1130, DOI: 10.2174/138945011795906615.

31 A. Cammarata, J. Marino, M. N. Atia, H. Duran and R. J. Glisoni, Novel doxycycline gold nanoparticles via green synthesis using PEO-PPO block copolymers for enhanced radiosensitization of melanoma, *Biomater. Sci.*, 2025, **13**, 3223–3241, DOI: 10.1039/D5BM00253B.

32 C. M. Coeshott, S. L. Smithson, E. Verderber, A. Samaniego, J. M. Blonder, G. J. Rosenthal and M. A. Westerink, Pluronic F127-based systemic vaccine delivery systems, *Vaccine*, 2004, **22**, 2396–2405, DOI: 10.1016/j.vaccine.2003.11.064.

33 S. S. Shen and Y. W. Yang, Dynamics of antigen delivery and the functional roles of L121-adjuvant, *Vaccine*, 2015, **33**, 4341–4348, DOI: 10.1016/j.vaccine.2015.04.051.

34 A. Badiee, V. Heravi Shargh, A. Khamesipour and M. R. Jaafari, Micro/nanoparticle adjuvants for antileishmanial vaccines: present and future trends, *Vaccine*, 2013, **31**, 735–749, DOI: 10.1016/j.vaccine.2012.11.068.

35 I. K. Han, Y. B. Kim, H. S. Kang, D. Sul, W. W. Jung, H. J. Cho and Y. K. Oh, Thermosensitive and mucoadhesive delivery systems of mucosal vaccines, *Methods*, 2006, **38**, 106–111, DOI: 10.1016/j.ymeth.2005.10.003.

36 J. Todoroff, B. Ucakar, M. Inglese, S. Vandermarliere, C. Fillee, J. C. Renauld, K. Huygen and R. Vanbever, Targeting the deep lungs: Poloxamer 407 and a CpG oligonucleotide optimize immune responses to Mycobacterium tuberculosis antigen 85A following pulmonary delivery, *Eur. J. Pharm. Biopharm.*, 2013, **84**, 40–48, DOI: 10.1016/j.ejpb.2012.11.020.

37 M. Lamrayah, C. Phelip, R. Rovera, C. Coiffier, N. Lazhar, F. Bartolomei, E. Colomb, B. Verrier, C. Monge and S. Richard, Poloxamers Have Vaccine-Adjuvant Properties by Increasing Dissemination of Particulate Antigen at Distant Lymph Nodes, *Molecules*, 2023, **28**, 4778, DOI: 10.3390/molecules28124778.

38 C. H. Chen, Y. J. Lin, L. T. Cheng, C. H. Lin and G. M. Ke, Poloxamer-188 Adjuvant Efficiently Maintains Adaptive Immunity of SARS-CoV-2 RBD Subunit Vaccination through Repressing p38MAPK Signaling, *Vaccines*, 2022, **10**, 715, DOI: 10.3390/vaccines10050715.

39 J. Süli, Z. Benísek, D. Eliás, S. Svrcek, A. Ondrejková, R. Ondrejka and V. Bajová, Experimental squalene adjuvant. I. Preparation and testing of its effectiveness, *Vaccine*, 2004, **22**, 3464–3469, DOI: 10.1016/j.vaccine.2004.02.023.

40 C. B. Fox, S. L. Baldwin, T. S. Vedvick, E. Angov and S. G. Reed, Effects on immunogenicity by formulations of emulsion-based adjuvants for malaria vaccines, *Clin. Vaccine Immunol.*, 2012, **19**, 1633–1640, DOI: 10.1128/CVI.00235-12.

41 C. B. Fox, Squalene emulsions for parenteral vaccine and drug delivery, *Molecules*, 2009, **14**, 3286–3312, DOI: 10.3390/molecules14093286.

42 S. G. Sparg, M. E. Light and J. van Staden, Biological activities and distribution of plant saponins, *J. Ethnopharmacol.*, 2004, **94**, 219–243, DOI: 10.1016/j.jep.2004.05.016.

43 K. Chen, W. Wang, X. Zhang, M. Wang, Y. Liu and Y. Shi, Potentials of saponins-based adjuvants for nasal vaccines, *Front. Immunol.*, 2023, **14**, 1153042, DOI: 10.3389/fimmu.2023.1153042.

44 A. Y. Nadeem, A. Shehzad, S. U. Islam, E. A. Al-Suhaimi and Y. S. Lee, Mosquirix™ RTS,S/AS01 Vaccine Development, Immunogenicity, and Efficacy, *Vaccines*, 2022, **10**, 713, DOI: 10.3390/vaccines10050713.

45 U.S. Food and Drug Administration, *Shingrix*, https://www.fda.gov/vaccines-blood-biologics/vaccines/shingrix, accessed Jan 6, 2026.

46 European Medicines Agency, *Mosquirix – Opinion on Medicine for Use outside the EU*, https://www.ema.europa.eu, accessed Jan 6, 2026.

47 U.S. Food and Drug Administration, *Arexvy*, https://www.fda.gov/vaccines-blood-biologics/arexvy, accessed Jan 6, 2026.

48 M. A. Lacaille-Dubois, Updated insights into the mechanism of action and clinical profile of the immunoadjuvant QS-21: A review, *Phytomedicine*, 2019, **60**, 152905, DOI: 10.1016/j.phymed.2019.152905.

49 N. Garçon and M. Van Mechelen, Recent clinical experience with vaccines using MPL- and QS-21-containing adjuvant systems, *Expert Rev. Vaccines*, 2011, **10**, 471–486, DOI: 10.1586/erv.11.29.

50 J. N. Hutter, P. M. Robben, C. Lee, M. Hamer, J. E. Moon, K. Merino, L. Zhu, H. Galli, X. Quinn, D. R. Brown, E. Duncan, J. Bolton, X. Zou, E. Angov, D. E. Lanar, M. Rao, G. R. Matyas, Z. Beck, E. Bergmann-Leitner, L. A. Soisson, N. C. Waters, V. Ngauy, J. Regules and S. Dutta, First-in-human assessment of safety and immunogenicity of low and high doses of Plasmodium falciparum malaria protein 013 (FMP013) administered intramuscularly with ALFQ adjuvant in healthy malaria-

naïve adults, *Vaccine*, 2022, **40**, 5781–5790, DOI: 10.1016/j.vaccine.2022.08.048.

51 V. A. Stewart, S. M. McGrath, D. S. Walsh, S. Davis, A. S. Hess, L. A. Ware, K. E. Kester, J. F. Cummings, J. R. Burge, G. Voss, M. Delchambre, N. Garçon, D. B. Tang, J. D. Cohen and D. G. Heppner, Preclinical evaluation of new adjuvant formulations to improve the immunogenicity of the malaria vaccine RTS,S/AS02A, *Vaccine*, 2006, **24**, 6483–6492, DOI: 10.1016/j.vaccine.2006.06.033.

52 N. Garçon, J. Silvano, C. F. Kuper, N. Baudson, C. Gerard, R. Forster and L. Segal, Nonclinical safety evaluation of repeated intramuscular administration of the AS15 immunostimulant combined with various antigens in rabbits and cynomolgus monkeys, *J. Appl. Toxicol.*, 2016, **36**, 238–256, DOI: 10.1002/jat.3167.

53 C. R. Alving, K. K. Peachman, G. R. Matyas and M. Z. Rao Beck, Army liposome formulation (ALF) family of vaccine adjuvants, *Expert Rev. Vaccines*, 2020, **19**, 279–292, DOI: 10.1080/14760584.2020.1745636.

54 M. Coccia, C. Collignon, C. Hervé, A. Chalon, I. Welsby, S. Detienne, M. J. van Helden, S. Dutta, C. J. Genito, N. C. Waters, K. Van Deun, A. K. Smilde, R. A. van den Berg, D. Franco, P. Bourguignon, S. Morel, N. Garçon, B. N. Lambrecht, S. Goriely, R. Van Most and A. M. Didierlaurent, Cellular and molecular synergy in AS01-adjuvanted vaccines results in an early IFNγ response promoting vaccine immunogenicity, *npj Vaccines*, 2017, **2**, 25, DOI: 10.1038/s41541-017-0027-3.

55 D. J. Marciani, Elucidating the mechanisms of action of saponin-derived adjuvants, *Trends Pharmacol. Sci.*, 2018, **39**, 573–585, DOI: 10.1016/j.tips.2018.03.005.

56 R. Marty-Roix, G. I. Vladimer, K. Pouliot, D. Weng, R. Buglione-Corbett, K. West, J. D. MacMicking, J. D. Chee, S. Wang, S. Lu and E. Lien, Identification of QS-21 as an inflammasome-activating molecular component of saponin adjuvants, *J. Biol. Chem.*, 2016, **291**, 1123–1136, DOI: 10.1074/jbc.M115.683011.

57 H. X. Sun, Y. Xie and Y. P. Ye, Advances in saponin-based adjuvants, *Vaccine*, 2009, **27**, 1787–1796, DOI: 10.1016/j.vaccine.2009.01.091.

58 E. Oliveira-Freitas, C. P. Casas, G. P. Borja-Cabrera, F. N. Santos, D. Nico, L. O. Souza, L. W. Tinoco, B. P. da Silva, M. Palatnik, J. P. Parente and C. B. Palatnik-de-Sousa, Acylated and deacylated saponins of Quillaja saponaria mixture as adjuvants for the FML-vaccine against visceral leishmaniasis, *Vaccine*, 2006, **24**, 3909–3920, DOI: 10.1016/j.vaccine.2006.02.034.

59 M. F. Bachmann and G. T. Jennings, Vaccine delivery: a matter of size, geometry, kinetics and molecular patterns, *Nat. Rev. Immunol.*, 2010, **10**, 787–796, DOI: 10.1038/nri2868.

60 D. Pineda Tenor, C. Martínez Laborde, A. Menchén Herreros and E. Fernández Rodríguez, Mathematical approach to correct the influence of hemolysis in common clinical laboratory tests, *Revista del Laboratorio Clínico*, 2010, **3**, 25–30, DOI: 10.1016/j.labcli.2009.07.004.

61 I. Smith, G. J. McCallum, A. V. Sabljic, J. I. Marfía, S. S. Bombicino, A. Trabucchi, R. F. Iacono, J. M. Birenbaum, S. C. Vazquez, J. M. Minoia, O. Cascone, M. G. López, O. Taboga, A. M. Targovnik, F. J. Wolman, M. Fingermann, L. G. Alonso, S. N. Valdez and M. V. Miranda, Rapid and cost-effective process based on insect larvae for scale-up production of SARS-CoV-2 spike protein for serological COVID-19 testing, *Biotechnol. Bioeng.*, 2021, **118**, 4129–4137, DOI: 10.1002/bit.27889.

62 A. Trabucchi, S. S. Bombicino, J. I. Marfía, A. V. Sabljic, R. F. Iacono, I. Smith, G. J. McCallum, A. M. Targovnik, F. J. Wolman, M. Fingermann, L. G. Alonso, M. V. Miranda and S. N. Valdez, Novel bridge multi-species ELISA for detection of SARS-CoV-2 antibodies, *J. Immunol. Methods*, 2022, **511**, 113365, DOI: 10.1016/j.jim.2022.113365.

63 M. O. Mohsen, M. D. Heath, G. Cabral-Miranda, C. Lipp, A. Zeltins, M. Sande, J. V. Stein, C. Riether, E. Roesti, L. Zha, P. Engeroff, A. El-Turabi, T. M. Kündig, M. Vogel, M. A. Skinner, D. E. Speiser, A. Knuth, M. F. Kramer and M. F. Bachmann, Vaccination with nanoparticles combined with micro-adjuvants protects against cancer, *J. Immunother. Cancer*, 2019, **7**, 114, DOI: 10.1186/s40425-019-0587-z.

64 Y. Yi, M. Yu, W. Li, D. Zhu, L. Mei and M. Ou, Vaccine-like nanomedicine for cancer immunotherapy, *J. Controlled Release*, 2023, **355**, 760–778, DOI: 10.1016/j.jconrel.2023.02.015.

65 J. Zhou, A. V. Kroll, M. Holay, R. H. Fang and L. Zhang, Biomimetic nanotechnology toward personalized vaccines, *Adv. Mater.*, 2020, **32**, e1901255, DOI: 10.1002/adma.201901255.

66 U.S. Food and Drug Administration, *Nuvaxovid COVID-19 Vaccine, Adjuvanted*, https://www.fda.gov/vaccines-blood-biologics/vaccines/nuvaxovid, accessed Jan 21, 2026.

67 K. Lövgren Bengtsson, B. Morein and A. D. Osterhaus, ISCOM technology-based Matrix-M™ adjuvant: success in future vaccines relies on formulation, *Expert Rev. Vaccines*, 2011, **10**, 401–403, DOI: 10.1586/erv.11.25.

68 H. X. Sun, Y. Xie and Y. P. Ye, ISCOMs and ISCOMATRIX™, *Vaccine*, 2009, **27**, 4388–4401, DOI: 10.1016/j.vaccine.2009.05.032.

69 S. Thakral, C. Levesque, K. Cung, L. Li, R. E. Mould, E. Moussa, J. Pinkstaff, G. Crotts, M. Slobodanka and Y. Krishnamachari, A pharmaceutical industry survey on exploring polysorbate alternatives in biological drug products: Poloxamer and other surfactants, *J. Pharm. Sci.*, 2025, **114**, 103917, DOI: 10.1016/j.xphs.2025.103917.